

Department of Precision and Microsystems Engineering

A Large Stroke Load-Carrying Member:
Towards the Design of a Load-Carrying Exoskeleton

K.K.H. Lam

Report no : 2018.015
Coach : Ir. W.W.P.J. van de Sande
Professor : Prof. dr. ir. J.L. Herder
Specialisation : Mechatronic System Design
Type of report : Master Thesis
Date : 11 July 2018

A Large Stroke Load-Carrying Member

Towards the Design of a Load-Carrying Exoskeleton

by

K.K.H. Lam

in partial fulfillment of the requirements for the degree of

Master of Science
in Mechanical Engineering

at the Delft University of Technology,
to be defended publicly on Wednesday July 11, 2018 at 10:00 AM.

Student number:	4172418	
Project duration:	June, 2017 – July, 2018	
Supervisor:	Prof. dr. ir. J. L. Herder	
Thesis committee:	Dr. ir. J. M. Kuiper,	TU Delft
	Ir. W. W. P. J. van de Sande,	TU Delft, coach
	Ir. R. Barents,	InteSpring BV

This thesis is confidential and cannot be made public until July 11, 2023.

An electronic version of this thesis is available at <http://repository.tudelft.nl/>.

Abstract

The company Intespring is currently developing a load-carrying exoskeleton for military personnel in order to reduce the impact of the ever increasing backpack load on their body: the Exobuddy. The current mechanical design gives rise to problems, i.e. the exoskeleton occupies a large space and applies torques on the legs of the user during operation, rendering it unsuitable for use in the field. This research is comprised of the redesign of the mechanical structure, where the functionality of the current exoskeleton is maintained, while eliminating the mentioned problems. The chosen solution, based on Storable Tubular Extendible Members (STEMs), is further developed and dimensioned according to a set of requirements. Finally a prototype is built to validate the design. It is shown that the proposed design is capable of carrying loads matching backpack loads of military personnel. Additionally, it is shown that the anisotropic material properties of Fibre Reinforced Composites can be exploited in such a way that a compact mechanism can be obtained.

Preface

This thesis marks the end of my career at the Delft University of Technology. I started as a Mechanical Engineering student at the faculty of Mechanical, Maritime and Materials Engineering. After obtaining my bachelor's degree, I continued my study career at the same faculty and chose the master program Precision and Microsystems Engineering, which I am graduating in now. I would like to take this opportunity to express my gratitude to everyone who has supported me during my time studying here.

I would like to thank Rogier for giving me the chance to write my thesis at InteSpring, a company full of great minds. I was also lucky enough to do my internship and even work for a brief period of time at InteSpring. Needless to say that I had a very enjoyable time there. I would like to thank everyone at InteSpring for their time, feedback during meetings and company. I would like to thank my daily supervisor Werner for his guidance and sparking new ideas in my head during our meetings. I would like to thank Just for his feedback and keeping me on the right track by asking the right questions. I would like to thank Mike for always being available and teaching me everything about the Exobuddy. I would like to thank Patrick and Harry for helping me conduct my experiments and thinking along. I would like to thank Johnny for always being there, listening to my rants and allowing me to keep a bird's-eye view of the thesis. Finally, I would like to thank my fiancée Vivian for always being there for me, taking care of me and believing in me.

*K.K.H. Lam
Delft, April 2018*

Contents

1	Introduction	1
1.1	Background	1
1.2	State of the Art	1
1.3	Problem description	2
1.4	Research Goal	3
1.5	Scope	3
1.6	Outline	3
2	Conceptual Design	4
2.1	Requirements and Constraints	4
2.1.1	Envisioned Use	4
2.1.2	Requirements	4
2.1.3	Working principle Exobuddy	5
2.1.4	Functional Analysis	7
2.2	Concept Generation	9
2.3	Evaluation	11
2.4	Final Concept	13
3	Dimensional Design	14
3.1	Assessment Criteria	14
3.2	Background	14
3.3	In-depth working principle	15
3.4	STEM Structure	17
3.5	Coiling Drum	19
3.6	Guidance Rollers	20
3.7	Balancing Spring	21
3.8	Rotary Damper	21
3.9	Expected Performance	22
4	Evaluation	23
4.1	Prototype	23
4.1.1	STEM	23
4.1.2	Side Plates	25
4.1.3	Coiling Drum	25
4.1.4	Guidance Rollers and Spacer Rods	25
4.2	Experiments and Results	26
4.2.1	Experiment 1	26
4.2.2	Experiment 2	29
4.2.3	Experiment 3	30
4.2.4	Prototype performance	30
5	Discussion	33
6	Conclusion	35
6.1	Future work	35

Bibliography	36
A Literature Review	38
B Material choice	68
C Composite material model	70
D Yielding	73
E Natural coiling radius	75
F Spring Choice	76
G STEM Fabrication	79
H Technical Drawings	82
H.1 Coiling Drum Drawing	83
H.2 Guidance Roller Drawing	84
H.3 Spacer Rod Drawing	85
H.4 Side Plate Drawing	86

1

Introduction

1.1. Background

Military personnel are often required to carry heavily loaded backpacks on their missions for extended periods of time. During a typical warfare operation soldiers are dispatched to a location distal to the point of interest, after which they manoeuvre towards it [1]. The backpacks, sometimes weighing in excess of 50 kg, generally are comprised of food, water, clothing, survival essentials, communication equipment and weaponry [2]. Studies have investigated the adverse effects of heavy military load carriage on the human body. These include acute injuries (foot blisters and lower back pain), chronic injuries (stress fractures, fatigue, knee pain and numbness of the upper body, otherwise known as “rucksack palsy”) and reduced tactical performance (mental alertness) [3]. The above mentioned consequences of heavy load carriage in turn result in high costs for the Ministry of Defence due to hospitalisation and early retirement of military personnel. In order to increase the success rate of the mission and decrease costs for the Ministry of Defence, it is imperative that soldiers are relieved from their heavy backpack loads.

Several possible solutions exist to relieve the soldiers from their heavy backpack loads. A straightforward solution is transferring the load to an auxiliary aid, such as a pack mule, cart or vehicle. While these solutions work well to decrease the load on the soldiers, the ground on which they operate is a critical point, as a relatively flat surface is necessary to advance. With hills and uneven ground during the mission, they are not the best suitable candidates.

A more modern solution is the use of load carrying exoskeletons. An exoskeleton is an externally worn device that serves to aid the wearer in some way, in this case carrying the load. Exoskeletons aim to work in concert with the wearer and are therefore, given their designated working environment, very suitable as a solution to relieve the soldiers from their heavy backpacks.

The company InteSpring is currently developing a load carrying exoskeleton for the load carriage problem at hand: the Exobuddy, shown in Fig. 1.1. It aims at becoming world’s lightest and most compact exoskeleton for load carriage. A unique feature of the Exobuddy is that it does not require external energy such as batteries to generate a supporting force. Only a small battery pack is necessary to power a control system.

1.2. State of the Art

Exoskeletons see use in a variety fields, e.g. medical, rehabilitation and military. In the medical field, exoskeletons such as the Indego and ReWalk [4, 5] enable mobility impaired people to perform everyday activities, e.g. walking and sitting. In the rehabilitation field, injured patients learn to move their limbs again through the use of exoskeletons like the Ekso GT [6]. Finally, in the military field, exoskeletons serve as devices that augment human capabilities, such as load carrying capacity and



Figure 1.1: The Exobuddy, designed to relieve soldiers from their heavy backpacks.

endurance. BLEEX [7], HULC [8] and XOS2 [9] are, similar to the Exobuddy, military focused exoskeletons. Exoskeletons can be categorised into the following categories: active, quasi-passive and passive. Active exoskeletons are powered, meaning they consume external energy (often electrical) to provide assisting forces. Passive exoskeletons do not require any external energy at all. Often times these exoskeletons are spring powered. Finally, quasi-passive exoskeletons do not require external energy to generate forces, however are powered in the sense that they require small amounts of energy to power their on-board control system. The Exobuddy belongs in the quasi-passive category. Active exoskeletons generally are capable of carrying heavy loads, however they are often heavy, bulky and consume large amounts of energy. Quasi-passive exoskeletons can carry similar loads, while being relatively light and consuming little energy, as supportive forces are generated passively. A more in-depth review on the state of the art of exoskeletons can be found in Appendix. [A](#)

1.3. Problem description

The Exobuddy succeeds in supporting a backpack load during walking. It also allows the user to squat and kneel down without colliding with the exoskeleton. However the Exobuddy occupies a large amount of space during operation, more specifically, the legs of the exoskeleton stick out to the sides significantly, giving rise to an increased risk of collision with obstacles, as depicted in Fig. 1.2. Additionally, during operation, the user experiences a torque on the feet, which induces the sensation as if the legs are forcibly rotated outward. These issues prevent the current Exobuddy from being usable in the military as soldiers are required to traverse through narrow spaces on their missions. Therefore it is necessary that the next iteration of the Exobuddy does not possess the above described issues.



Figure 1.2: The legs of the Exobuddy tend to rotate outward during operation, increasing the risk of collision with obstacles.

1.4. Research Goal

The goal of this research is to analyse the problem at hand and propose a redesign for the exoskeleton, where the occupied space is small (i.e. a close to body device) and the current functionality of the Exobuddy is preserved. To this end, a literature study on the state of the art of current exoskeletons was conducted, after which the redesign of the Exobuddy was approached in a systematic manner, as described by Pahl and Beitz [10].

1.5. Scope

This research will primarily be focused on the mechanical aspect of the Exobuddy. In particular, the mechanism that allows the backpack load to be transferred to the ground. As the goal is to design a quasi-passive exoskeleton, powered solutions are not considered. While a control system is present in the Exobuddy, it is not considered for the redesign.

1.6. Outline

Chapter 2 describes the conceptual design phase, where the requirements and constraints are determined. A functional analysis is performed in order to establish the key functions, after which solutions are generated through the use of a morphological chart. Several solutions are evaluated and a final concept is chosen.

In Chapter 3, the complete concept is first presented, after which the individual components of the mechanism are discussed and dimensioned.

Chapter 4 discusses the evaluation of the design. A prototype is built and experiments are conducted to validate the design. In Chapter 5, the results of the experiments are discussed and interpreted. Finally, this thesis will be concluded in Chapter 6.

2

Conceptual Design

A systematic design approach as described by Pahl and Beitz [10] was adopted towards the design of the device. Requirements are gathered in order to determine the functionality of the device. After obtaining the function structure, a morphological chart is used to generate concepts, which are evaluated and rated according to a number of evaluation criteria. Finally, a concept is chosen for further development.

2.1. Requirements and Constraints

2.1.1. Envisioned Use

The device is intended to partially unload military personnel from their heavy backpacks for extended periods of time during missions. In practice this means that the experienced load for the soldier should reduce when using the device. During usage, the soldier is able to carry out voluntary movements, such as walking, kneeling and squatting. During walking, the device is supporting a load, however when kneeling and squatting down, no load is required to be supported. In the case that the soldier encounters danger, the heavy backpack, including the device, is to be cast off, leaving a small backpack on the user's back.

2.1.2. Requirements

Requirements for the device are obtained from previous research and through discussion with researchers. Some requirements are not valid at the current stage of the device, and thus the device will not be evaluated according to every requirement. They are however still included as they may serve a good purpose as guidelines towards the design of the device. The list of requirements, alongside the values (if applicable) and the notion of whether it is a demand or a wish, is displayed in table 2.1.

Table 2.1: Requirements list

Requirement	Value	Demand/Wish
Functional		
Support backpack load during walking	>30kg	D
Does not buckle	>30kg	D
Damping of heel strike		W
Easy donning	<2min	W
Easy doffing	<15s	W
Allow walking RoM		D
Allow kneeling RoM		D
Allow squatting RoM		D
Operational on various grounds	mud, road, sand	W
Operational at various walking speeds	3 - 5km/h	W
Operational at various slopes		W
Operational for extended periods of time	72h continuously	W
Adaptable to different backpack loads	20 - 30kg	W
Adaptable to different users	P05 - P95 of population	W
Residual force at feet	<2kg	D
Energy		
No external energy source for support		D
Ergonomics		
Lightweight	<14kg	D
Low distal mass		W
Compact		W
Does not increase footprint of user		D
Low forces at interface between device and user		D
No sharp parts		D
Silent		W
Safety		
Quick release in case of emergency		W
May not injure user		D
May not collide with user		D
Close to body (Max. dimensions)	<200x344x1150mm	D
Manufacturing		
Low cost		W
Easy manufacturing		D

2.1.3. Working principle Exobuddy

Analysing the working principle of the Exobuddy will aid in conducting the functional analysis. We will restrict ourselves to a two-dimensional analysis of the working principle for the sake of simplicity and clarity.

A 2D linkage representation of the exoskeleton-human system is shown in Fig. 2.1. Some up and down sliding motion is permitted between the backpack and the user's back, however the backpack does not release from the back of the user, i.e. the backpack and the user are always in contact.

The exoskeleton consists of two bars connecting the backpack (point A) with the user's shoe (point C). The linkage in green essentially facilitates relative motion between points A and C. A controllable, linear, hydraulic damper is placed between the two bars, effectively acting as a rotational damper at point B. This mechanism can be simplified to a two bar mechanism with a prismatic joint, as shown in Fig. 2.2, where the linear damper directly acts as the prismatic joint.

By increasing the damping coefficient of the damper, resistance to motion is generated, and thus the backpack load can be transferred through the damper to the ground. By varying the damping coefficient appropriately, such that no damping is present when the leg is swung forward and high damping is present when the leg is on the ground, it is ensured that the load is carried during walking without obstructing the movements of the user.

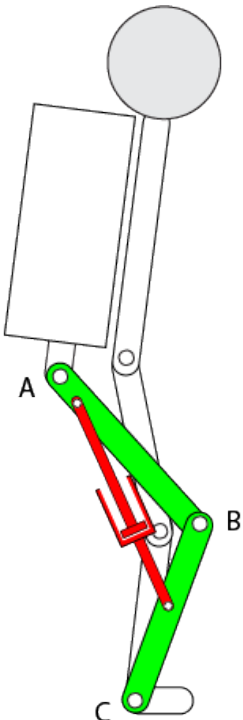


Figure 2.1: A linkage representation of a person equipped with the Exobuddy. Green: linkage structure, red: hydraulic damper. Note that only one leg is drawn here.

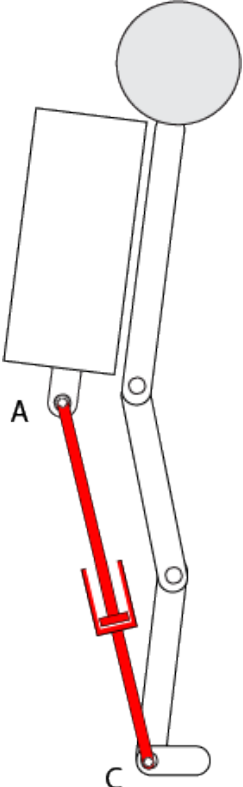


Figure 2.2: A simplified model of the Exobuddy.

2.1.4. Functional Analysis

In order to generate potential solutions for the design problem, the main function and sub-functions of the device are determined.

Functional approach

The exoskeleton should unload the musculoskeletal system of the user, thus the backpack load is to be transferred directly to the ground, bypassing the user's body. To this end, the exoskeleton should be able to carry a load, and therefore be able to transfer forces to the ground.

The exoskeleton should not hinder the user in its movements, i.e. walking, kneeling and squatting. Thus sufficient range of motion of the user is required.

Human walking is characterised by two alternating phases for each leg: stance and swing (refer to Appendix. A for further reading on human gait). During stance, the leg is in contact with the ground and a load is transferred to it, whereas during swing no load is transferred, as there is no contact with the ground. Similar to the human legs, the exoskeleton should transfer a load during stance phase and transfer no load during swing phase. A visualisation of the two phases of the gait cycle is presented in Fig. 2.3. It can be seen that a slight overlap in stance phase for both legs is present. During this period, both legs are in stance phase and the load transfer is switched from one leg to the other. Thus, a load is transferred to the ground at all times.

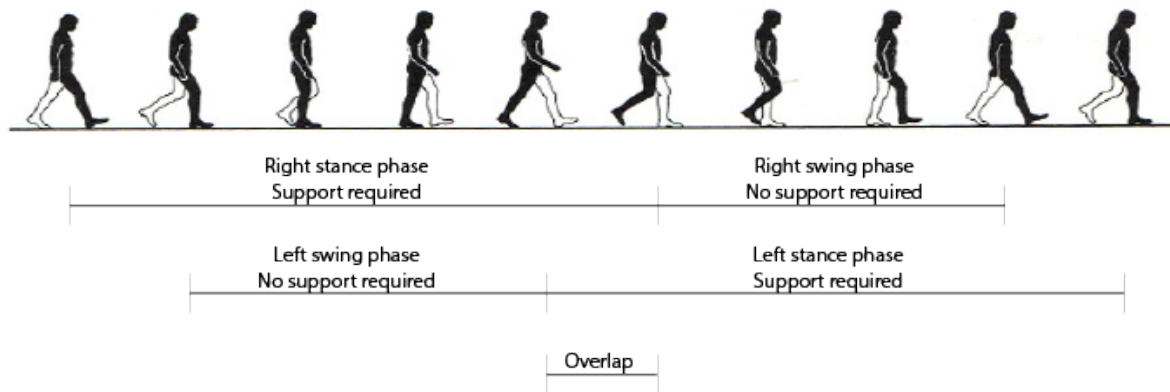


Figure 2.3: A side view of a gait cycle for the right leg. The legs in black and white correspond to the right and left legs, respectively. Heel strike marks the start of the gait cycle. It can be seen that at all times at least one leg is in stance.

Abstract approach

A different way to look at the matter is the following. During walking, distances between two arbitrary points on the body that are not lying on the same limb portion vary continuously. The backpack and ankle are two particularly interesting points, as they are the connection points for the exoskeleton. Fig. 2.4 shows the change in distance between the ankle and backpack during one gait cycle. Approximately, the first half of the gait cycle is the stance phase, whereas the second half is the swing phase. These figures are produced in MATLAB using kinematic gait data from Bovi et al. [11]. Fig. 2.5 gives a visualisation of the link model used to measure the distance. Based on the DINED anthropometric data for dutch male adults between 20 and 30 years old [12], the following limb lengths were used:

- Shank: 497mm
- Thigh: 586.5mm
- Foot: 269mm
- Hip to eyes: 688mm
- Distance backpack attachment point to hip: 150mm perpendicular to the torso

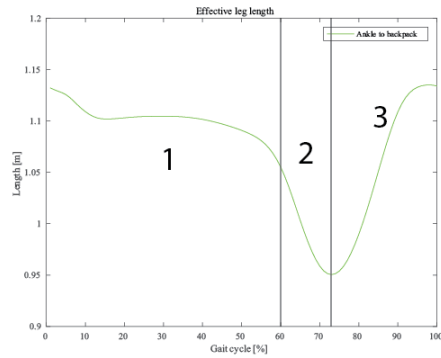


Figure 2.4: Distance between ankle and backpack during a single gait cycle. Three regions can be distinguished. 1: Load transfer during compression, 2: no load transfer during compression, 3: no load transfer during extension.

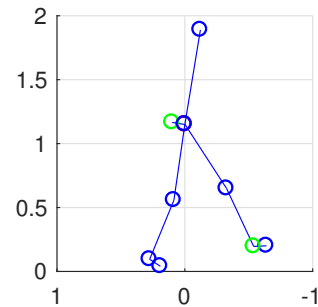


Figure 2.5: Link model of a human during walking. The two green circles represent the locations of the backpack attachment point and the ankle. For simplicity, the arms are omitted.

During the stance phase (0-60% of the gait cycle, region 1 in Fig. 2.4), the distance is primarily decreasing, suggesting that the device should be able to generate a force while undergoing compression. In practice, this could be seen as if the exoskeleton is slowing the backpack down during its descent.

During swing phase (60-100% of the gait cycle, regions 2 and 3 in Fig. 2.4), both shortening and extension take place, where no force is required to be transferred. This means that the device should be able to selectively provide a force or no force. Thus we can identify three working modes (also indicated in Fig. 2.4), namely:

1. Load transfer during compression
2. No load transfer during compression
3. No load transfer during extension

Between squatting and kneeling, the smallest distance between backpack and shoe occurs during kneeling. This distance serves as a lower bound for the length between the backpack and shoe. The value was obtained through measuring the distance between the backpack and shoe of colleagues in a kneeling position and taking the mean of the results. This amounted to a distance of 300mm.

In conclusion the redesign of the exoskeleton can be abstracted to the design of a device connecting two points that is capable of selectively generate a supportive force while undergoing a change in length. Furthermore, the length change should be sufficiently large that all the relevant motions of the user are allowed, i.e. walking, kneeling and squatting. The preceding analysis is summarised and visualised in Fig. 2.6.

It should be noted that only during walking, a supporting force is required. Fig. 2.7 is a visualisation of the range of length changes that the device should facilitate.

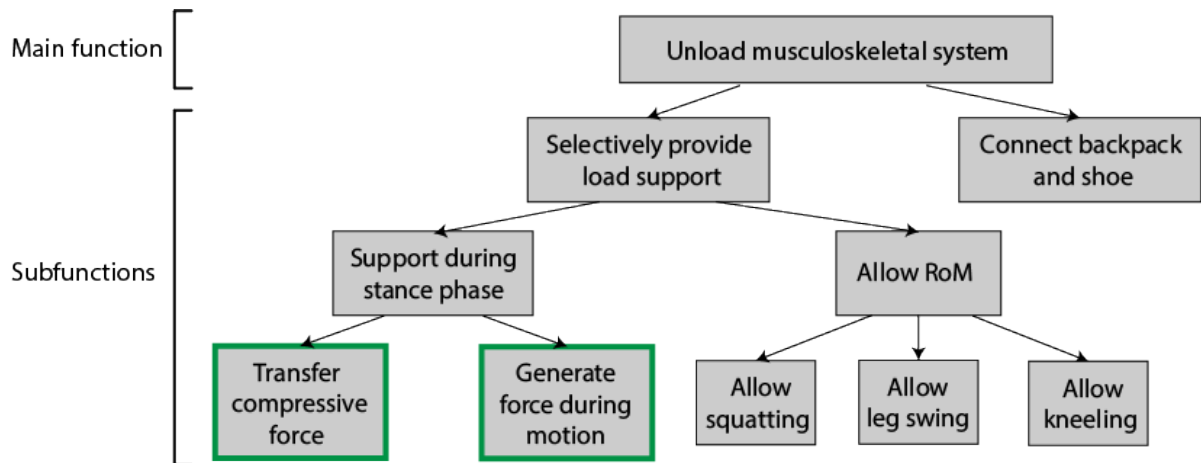


Figure 2.6: Function structure of the system



Figure 2.7: A visualisation of the range of lengths that the device should facilitate. The minimum length occurs while kneeling while the maximum length occurs when the leg just touches the ground during walking.

2.2. Concept Generation

Following the functional analysis, solutions to the two sub-function highlighted in green in Fig. 2.6 are generated and combined to develop possible concepts through the use of a morphological chart, shown in Fig. 2.8. The other sub-functions are omitted, as they are deemed too abstract to yield relevant sub-solutions. Instead they are used as evaluation in mind while searching for sub-solutions to the two chosen sub-functions. The solutions combined to generate concepts. In this section, the concepts will be elaborated on.

Sub-function Type	Transfer compressive force											
	Flexible					Rigid					Pressure	Magnetic
	Bowden cables	Singular linkage	Push-pull chain	Leaf spring	Linkage with lockable joints	Tape spring	Rigid link	Inflatable structure	Piston-cylinder	Magnets		
Solution												

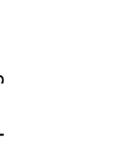
Sub-function Type	Generate force during motion								
	Mechanical				Hydraulic				Magnetic
	Compression spring	Torsion spring	Flywheel	Hydraulic piston-cylinder	Eddy-current brake	Magneto-rheological damper			
Solution									

Figure 2.8: Morphological chart for the sub-functions: Transfer compressive force and generate force during motion

Scissor concept

The working principle of this concept is based on a scissor-like linkage that connects the backpack with the user's shoe. The linkage acts as a prismatic joint, allowing motion of the leg. A variable rotary damper is added at the top joint, restricting/allowing rotation of the joint, and thereby restricting/allowing the extension and compression of the scissor linkage. Damping is turned on during the stance phase and turned off during the swing phase for each leg. By doing so, the backpack load is transferred to the ground during the stance phase and the leg is free to be swung forward during the swing phase.

Telescopic cylinder concept

This concept comprises a telescopic cylinder connecting the backpack and the user's shoe. A telescopic cylinder is a cylinder-piston type device with multiple cylinders. Each subsequent cylinder is smaller than the previous one, such that they are capable of being nested within each other. This gives rise to a structure with a significant extended to retracted length ratio. Damping is generated hydraulically.

Anthropomorphic concept

The following concept is based on the human leg and the most widely used type for exoskeletons. Similar to the human leg, this concept is comprised of an upper and lower leg, connected via a knee joint. The knee joint facilitates the distance change between the backpack and ankle. By implementing a damping element at the knee joint, for example, a rotary damper or a linear damper connected between the upper and lower leg, the backpack can be supported.

Tape measure concept

This concept incorporates a tape measure-like structure. Tape measures possess the convenient capability of rolling up very compactly and extending significantly. A custom designed tape measure that is stiff enough to serve as a structural element is attached between the backpack and shoe. Coiling and uncoiling of the tape measure results in a prismatic connection between the backpack and shoe, allowing the user to walk, kneel and squat. Support during stance phase is provided by means of a rotary damper attached to the drum on which the tape measure is coiling on.

Linear damper + locked knee concept

This concept combines a linear damper with a linkage similar to the human leg: an upper and lower leg and a knee joint. The knee joint is lockable by means of a ratchet. During walking, the knee joint remains locked, resulting in a rigid structure, while the linear damper exerts a force to support the backpack. Solely a linear damper does not provide sufficient range of motion of the legs for kneeling and squatting due to the minimum length of the damper. To overcome this issue, the knee joint unlocks when squatting and kneeling is necessary.

2.3. Evaluation

The preceding concepts are evaluated according to a number of evaluation criteria based on the design requirements list. The requirements that are deemed most important are used as a basis for the evaluation criteria, listed and if necessary elaborated on below. The criteria are given weighting factors of 1, 1.5 or 2, indicating least important, fairly important and very important, respectively.

Complexity A weighting factor of 1.5 has been given to the complexity of the concept. It is important to get a feel of the complexity for the feasibility and further development of the concept. Complex concepts get a low score, whereas simple concepts get a high score.

Close to body With regard to acceptance by the end user, it is important that the exoskeleton is as close to the body as possible. Having many components distal to the body increases the risk of collision with obstacles or other body parts during operation. A weighting factor of 2 has been given. The closer to the body a concept is, the higher the score.

Low distal mass Distal mass in this context is defined as the mass located far away from the centre of mass of the user. It is thought that high distal mass increases torques required by the joints to swing the leg forward. A weighting factor of 1.5 is applied for this criterion. Concepts with low distal mass score high, whereas concepts with high distal mass score low.

Easy donning and doffing Easy donning and doffing is required for the final product, however it is not deemed necessary for the current phase. Therefore the potential of easy donning and doffing is evaluated. A weighting factor of 1 is given due to the relatively low importance at this stage.

Number of components The number of components should be kept low in order to reduce cost and allow for an efficient system with little friction. A weighting factor of 2 is given.

Ease of prototyping For the sake fast fabrication of a prototype, the concept should be somewhat easily producible. However, this criterion should not become a basis for the choice of the final concept, therefore a weighting factor of 1 is given.

Risk of injury The exoskeleton should be pose a potential risk of injury to the user. Since safety is of utmost importance, this criterion is given a weighting factor of 2. Safe concepts score high, whereas dangerous concepts score low.

Lightweight Lightweight equipment in the military is an important aspect when evaluating concepts. However it is not a priority at the current stage as subsequent design iterations are expected to make the product more weight efficient. A weighting factor of 1 applies for this criterion.

Low cost Cost of the product is not an important criterion at this stage, however it should be taken into account when evaluating concepts. A weighting factor of 1 is applied. Low cost concepts score high, whereas high cost concepts score low.

As not every criterion has an equal importance, weighting factors are used. Furthermore a scale from 0 to 4 is used, where 0 is worst and 4 is best. This scale is chosen, because a scale from 0 to 10 would suggest a higher accuracy on the assigned evaluation values than what is actually present at the current stage. Values are assigned based on common knowledge and intuition. The evaluation of the concepts is presented in Table 2.2.

Table 2.2: Evaluation of concepts, the scores are multiplied by the corresponding weighting factor, summed up and normalised

Criteria	Weighting factor	Scissor concept	Telescopic cylinder concept	Damped knee concept	Tape measure concept	Linear damper + locked knee concept
Complexity	1.5	2	3	3	2	2
Close to body	2	2	2	3	3	3
Low distal mass	1.5	2	3	2	4	2
Low interface forces	1.5	4	4	3	4	3
Easy donning and doffing	1	2	3	2	3	2
Number of components	2	2	2	2	3	1
Ease of prototyping	1	3	2	3	3	3
Risk of injury	2	1	3	3	2	2
Lightweight	1	2	2	3	3	3
Low cost	1	2	2	3	2	2
Normalised total score		0.53	0.66	0.67	0.72	0.56

2.4. Final Concept

The tape measure concept has a highest score of 0.72, followed by the telescopic cylinder concept and the damped knee concepts with scores of 0.66 and 0.67, respectively. These are the three most promising concepts. Based on the highest score and novelty of the concept, the tape measure concept is chosen as a final concept. An impression of the concept can be found in Fig. 2.9.

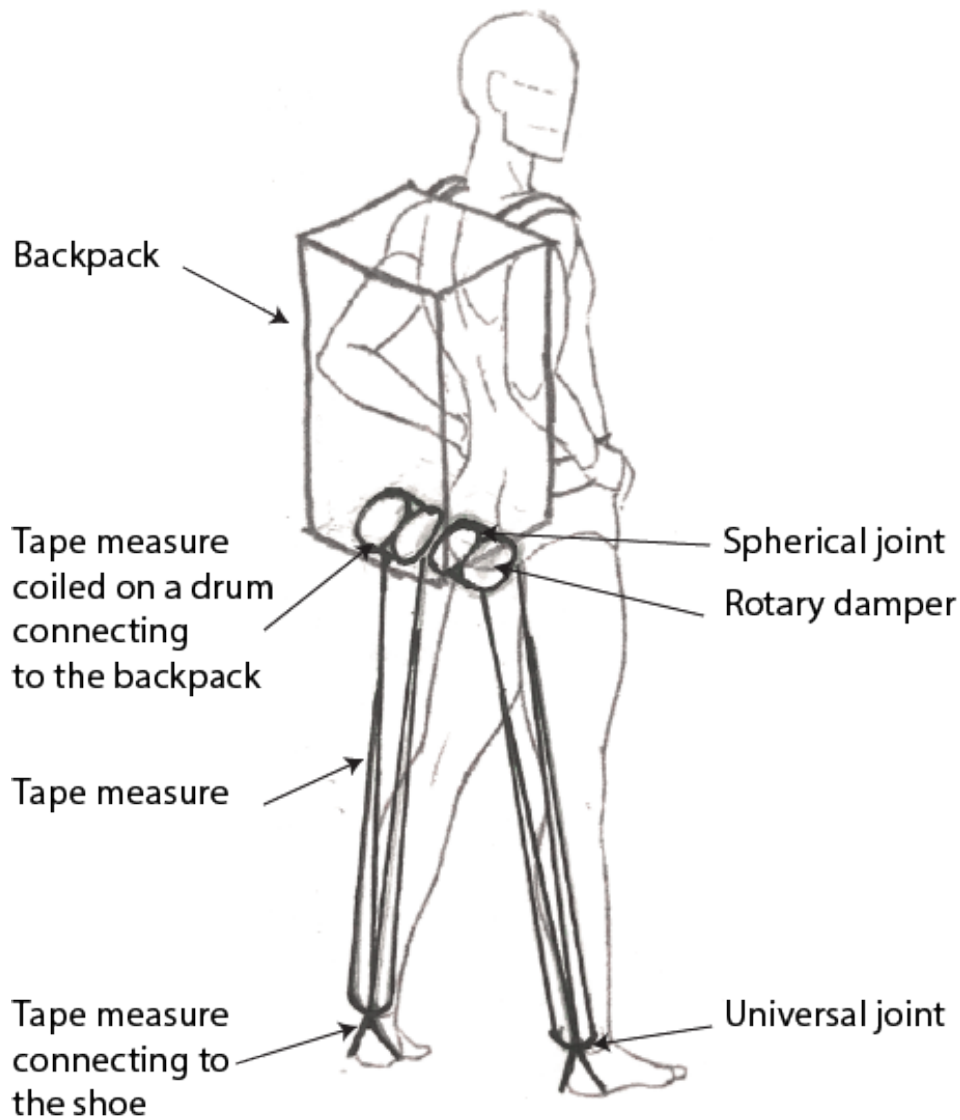


Figure 2.9: A sketch of the final concept

3

Dimensional Design

Having chosen the final concept, the design can be worked out in more detail. The concept is based on a tape measure. The metal strip inside a tape measure is a so-called tape spring. In this chapter, a tangible requirements list is presented in order to assess the final design, some background on tape springs is provided, an in-depth explanation of the concept is given and thereafter each component of the concept is individually dimensioned.

3.1. Assessment Criteria

In order to assess validate whether the design will fulfil the requirements in Table 2.1, they are translated into tangible criteria. They are presented below:

Table 3.1: Requirements for assessment

Requirement	Desired Value
Support backpack load during walking	>300N
Does not buckle	>300N
Residual force at feet	<20N
Lightweight	<14kg
Close to body (Max. dimensions)	<200x344x1150mm
Distance between backpack and shoe	min. 300mm, max. 1150mm

3.2. Background

Tape springs are a type of compliant mechanism possessing the convenient capability of being folded and coiled elastically. In their unstressed state, they can be regarded as straight, thin-walled beams with an open, circular cross-sections. Fig. 3.1 shows a typical tape spring along with its dimensions. Here, α , R , h and L are the subtended angle, radius of curvature, thickness and length, respectively.

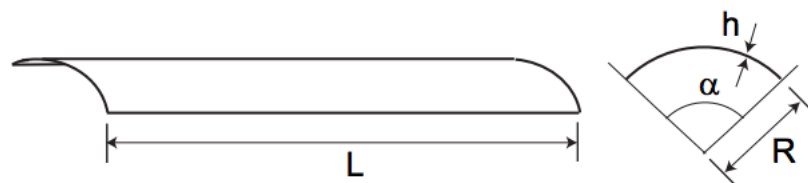
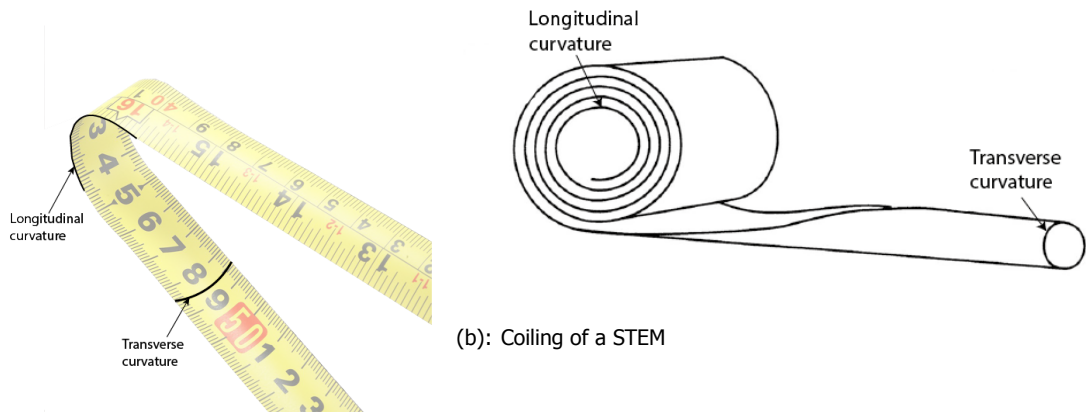


Figure 3.1: A typical tape spring and its dimensions

The process of folding and coiling of a tape spring is characterised by flattening of the initial transverse curvature and subsequently introducing a longitudinal curvature. Folding of a simple tape measure and coiling of a STEM are shown in Fig. 3.2.



(a): Bending of a tape measure

(b): Coiling of a STEM

Figure 3.2: Examples of folding and coiling of tape spring structures. Longitudinal and transverse radii of curvature are referred to by r_x and r_y , respectively.

Typically, tape springs are fabricated from metal, however in recent history, composite materials are seeing more use for the fabrication of tape springs [13]. Bending of tape springs stores elastic energy due to the deformation. The capability of being folded and coiled of tape springs can be exploited in a number of ways. Tape springs primarily see use in aerospace industry due to the compactness of the folded or coiled state. They are used as hinges and booms for deployable structures, such as antennas and solar panels for satellites [14–17]. Generally, tape springs subtend angles smaller than 180° . A special type of tape spring is the STEM, a Storable Tubular Extendible Member, which subtends an angle of 360° or more, originally invented by George Klein in 1951 [18].

3.3. In-depth working principle

As established in Sec. 2.1.4, the device should form a connection between the backpack and shoe of the user in order to transfer loads to the ground. To this end a concept inspired by the working principle of a tape measure was chosen. A schematic overview of the working principle of the concept is presented in Fig. 3.3. A 3D render of the top part of the mechanism where the STEM is omitted, is shown in Fig. 3.4.

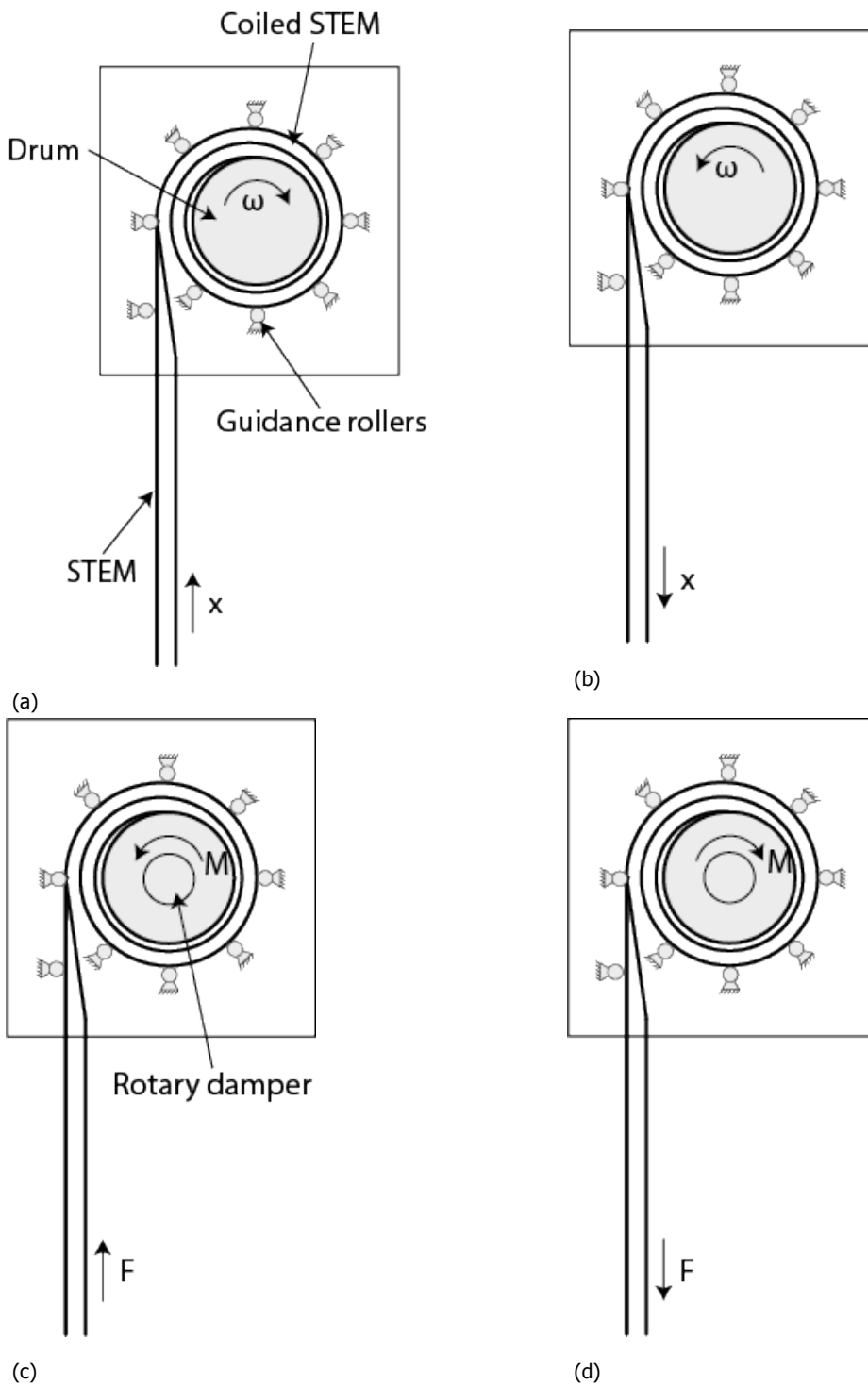


Figure 3.3: Working principle depicted in various working conditions. (a): As the STEM is compressed, the drum and coil rotate, such that the STEM coils up. (b): As the STEM is extended, the drum and coil rotate, such that the STEM uncoils. (c,d) The rotary damper exerts a counter moment M , resisting the force F . For clarity, the rotational balancing spring is not drawn here.

The STEM, which is fixed to the drum, serves as a structural element for load transfer. The top part of the device is attached to the bottom of the backpack through a spherical joint and the bottom of the device is connected to a shoe mount through a universal joint. The cross section of the STEM end that connects to the shoe mount is kept tubular in order to maintain a high bending stiffness.

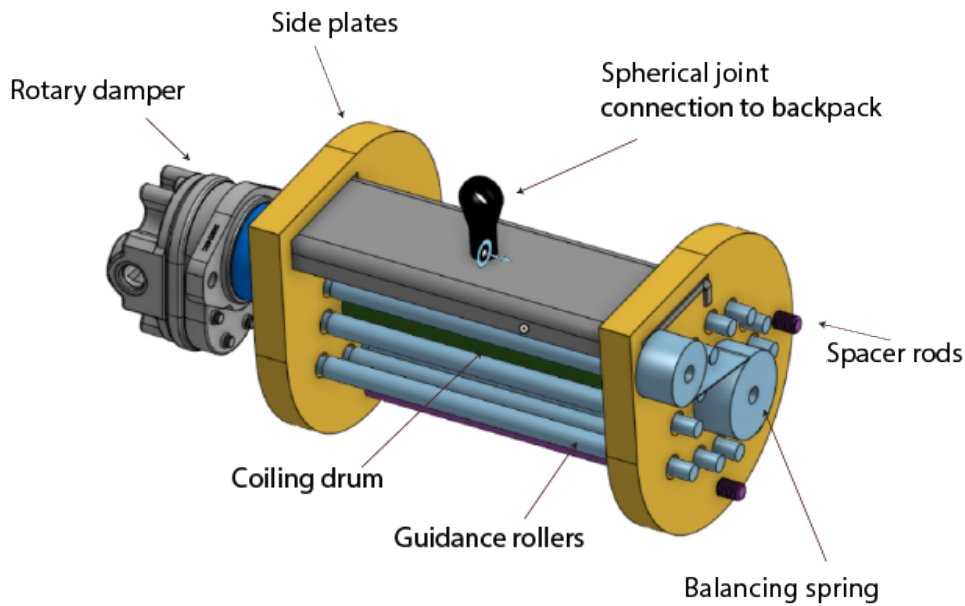


Figure 3.4: Render of the top part of the mechanism. The STEM is not shown here.

As the STEM is compressed and extended during walking, it coils and uncoils onto the drum as visualised in Figs. 3.2(a) and 3.2(b). The drum, in turn is connected to a controllable, rotary damper. By activating the damper, rotation of the drum is resisted, which in turn resists compression and extension of the STEM, allowing a load to be transferred, shown in Figs. 3.2(d) and 3.2(c).

As the STEM is coiled onto the drum, strain energy is stored. In order to release the strain energy, the STEM will have a tendency to return to its original state, thus uncoiling and extending the STEM. To counteract this tendency to uncoil, a rotational spring is attached to the axis of the drum.

Furthermore, guidance rollers are placed around the drum in order to contain the STEM in its coiled position.

The concept described above in essence provides a linear motion which can be damped. As such, we can view the mechanism as a linear controllable damper with a large stroke to free length ratio when regarding its purpose in the design of a load carrying exoskeleton.

The major components of the mechanisms are:

- STEM structure
- Coiling drum
- Guidance rollers
- Balancing spring
- Rotary damper

3.4. STEM Structure

The main purpose of the STEM structure is to serve as a structural element for load transfer, while also being coil-able onto a drum. Sizing of the remaining components depends largely on the dimensions of the STEM. As the STEM acts as a load-carrying column in this concept, one of the failure mechanisms is column buckling. The STEM should not buckle under the influence of the load of the backpack. Furthermore, as the STEM is coiled onto a drum, significant strain is imparted on the material, thus another failure mechanism is yielding of the material. The strain due to coiling should not exceed the maximum admissible strain of the material. The final STEM should not fail by the two mentioned failure mechanisms.

In order to start dimensioning the STEM, it is convenient to select a material first. The material choice procedure, detailed in Appendix. B, resulted in Glass-Fiber-Reinforced Composites (GFRC).

Euler's buckling criterion for column buckling is given by

$$F_{crit} = \frac{\pi^2 EI}{4L^2} \quad (3.1)$$

, where E , I and L are the Young's modulus, second moment of inertia and length of the STEM, respectively. For I , a tubular cross section is taken, given by

$$I = \frac{\pi}{4}((r_y + t)^4 - r_y^4) \quad (3.2)$$

, where r_y and t are the transverse radius of curvature and the thickness of the STEM. We can vary E , r_y and t in order to maximise the critical load.

The maximum strain imparted on the STEM as a result of coiling is given by

$$\epsilon_y = \frac{t}{2r_y} \quad (3.3)$$

The derivation of Eq. (3.3) is given in Appendix. D. r_y has the greatest effect on I (thus also on F_{crit}), as it is generally much larger than t . Therefore r_y is dimensioned first and t is tweaked such that the maximum strain of the material is not exceeded.

The maximum admissible strain for GRFCs was taken to be 2%. Fig. 3.5 shows a plot of allowable combinations of thickness and radius of curvature.

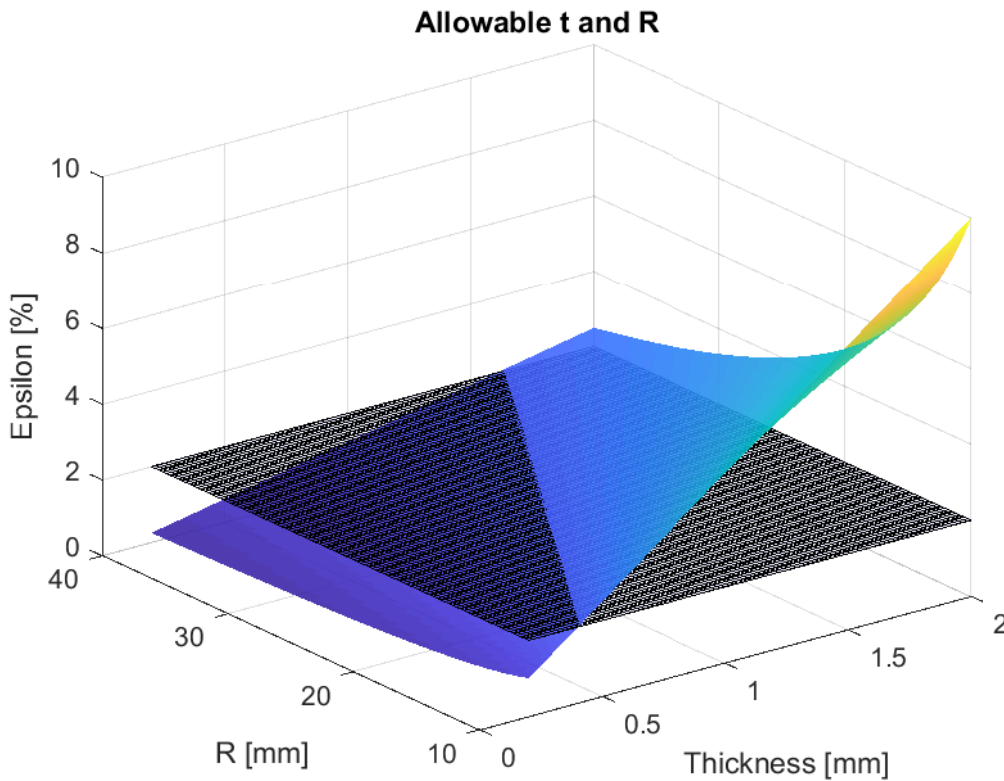


Figure 3.5: Surface plot of allowable combinations of thickness t and radius of curvature R . The surface in black indicates the upper bound of 2% strain.

Taking into account the available space under the backpack, a transverse radius r_y of 25mm was chosen, combined with a thickness t of 0.6mm. The Young's modulus was obtained from a material model based on Classical Laminate Theory, shown in Appendix. C. These values amounted to a critical load of 394N and a maximum strain of 1.2%, both satisfying the required values.

3.5. Coiling Drum

The coiling drum allows the STEM to be coiled onto it and for torques to be transmitted between the damper and the STEM. In order to reduce unwanted friction between the guidance rollers and the STEM as it is coiling and uncoiling, it is desired that the STEM makes no contact with the guidance rollers, during free extension and compression, when no support is necessary. Additionally, a coiling drum with a small radius will contribute to a compact and lightweight system.

Coiling a STEM introduces a certain, preferred, longitudinal radius of curvature, referred to as the natural coiling radius, r_{xn} . This natural coiling radius is a result of an energy minimum at this state. The relationship between the transverse radius r_y and r_{xn} (derived in Appendix. E), is given by

$$r_{xn} = \sqrt{\frac{D_{11}}{D_{22}}} r_y \quad (3.4)$$

, where D_{11} and D_{22} are entries of the material bending stiffness matrix D , obtained from the material model presented in Appendix. C. By choosing a drum radius greater than r_{xn} , the STEM will have a tendency to clamp itself onto the drum, and thus avoid making contact with the guidance rollers. For isotropic materials, such as steel, D_{11} and D_{22} are equal and therefore r_{xn} and r_y are equal, suggesting that the smallest drum radius where this clamping behaviour is present would have to be greater than r_y . However for anisotropic materials, such as GRFCs, this is not the case. It turns out that the entries of the D matrix are dependent on lay up of the composite laminate. More specifically, the D matrix is dependent on the fibre orientation angle of the layers. By choosing the fibre orientation angles such that $\sqrt{\frac{D_{11}}{D_{22}}} < 1$, it is possible to obtain a natural coiling radius smaller than the transverse radius. This allows for the choice of a drum radius smaller than r_y , resulting in a compact system with minimal friction during free extension and compression of the STEM. Choosing a fibre orientation angle of 60° results in a D matrix ratio of $\sqrt{\frac{D_{11}}{D_{22}}} = 0.57$. Combined with the value of 25mm obtained in Sec. 3.4 for r_y , results in a natural coiling radius r_{xn} of $0.57 \cdot 25 = 14.37\text{mm}$.

From a compactness point of view, one could argue that choosing a drum radius slightly larger than r_{xn} is the best choice. However, a number of additional aspects should be taken into account when choosing the drum radius. It should be noted that the guidance rollers are to be placed in a way such that sufficient space between them and drum is reserved for the STEM to coil up significantly during keeling and squatting of the user. Fig. 3.6 shows the radius increase of the drum as a STEM is coiled onto it for various drum radii.

The smaller the drum radius, the larger the radius increase becomes when coiling the STEM, implying that for smaller drum radii, the reserved space between the drum and guidance rollers becomes larger. This increases play in the system when engaging the damper, as the STEM has more room to blossom, which is undesirable. Blossoming occurs when the STEM is compressed, while a counteracting torque is restricting the drum from rotating freely. As the drum is unable to rotate, the STEM will release and expand away from the drum, i.e., blossom, as shown in Fig. 3.7.

Additionally, as the STEM is compressed and thus coiled onto the drum, strain energy is stored in the material, resulting in a spring-like behaviour of the STEM, i.e., the STEM will have a tendency to uncoil and extend in order to restore back to its preferred state. This behaviour is undesired from a comfort point of view, as retraction of the leg will be resisted, while extension is assisted.

Approximating the coiling of the STEM onto a drum as an Archimedean spiral and using an energy method, as presented by Hoskin et al. [19], we can obtain the force displacement curves of the STEM for various drum radii. Fig. 3.8 shows the resulting force-displacement curves. It can be seen that for $r_{drum} = 25\text{mm}$ and 30mm , the force displacement characteristics are near constant along the displacement. The resulting forces are also lowest for these radii. Finally, a drum radius of 25mm was chosen as it results in a low, fairly constant force-displacement behaviour. The drum was chosen to be made of aluminium for ease of prototyping. Due to relatively large radius, it is not expected to deform significantly.

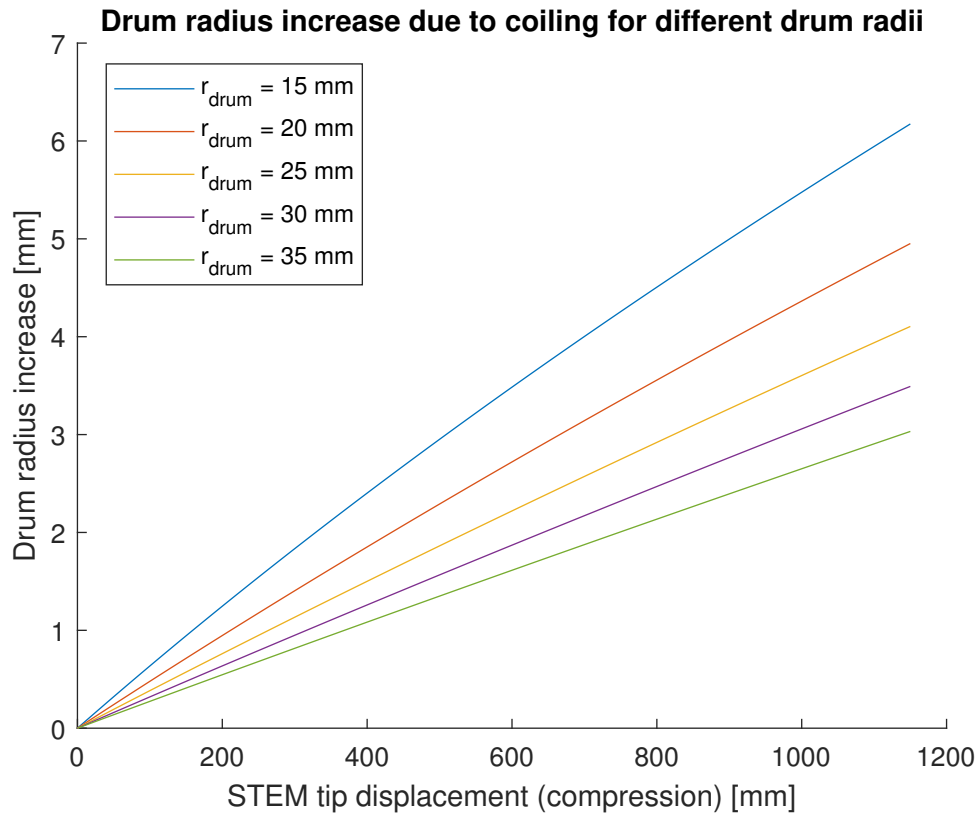


Figure 3.6: Increase in radius as a result of coiling the STEM for various drum radii. The smaller the drum radius, the larger the total increase in radius will be.

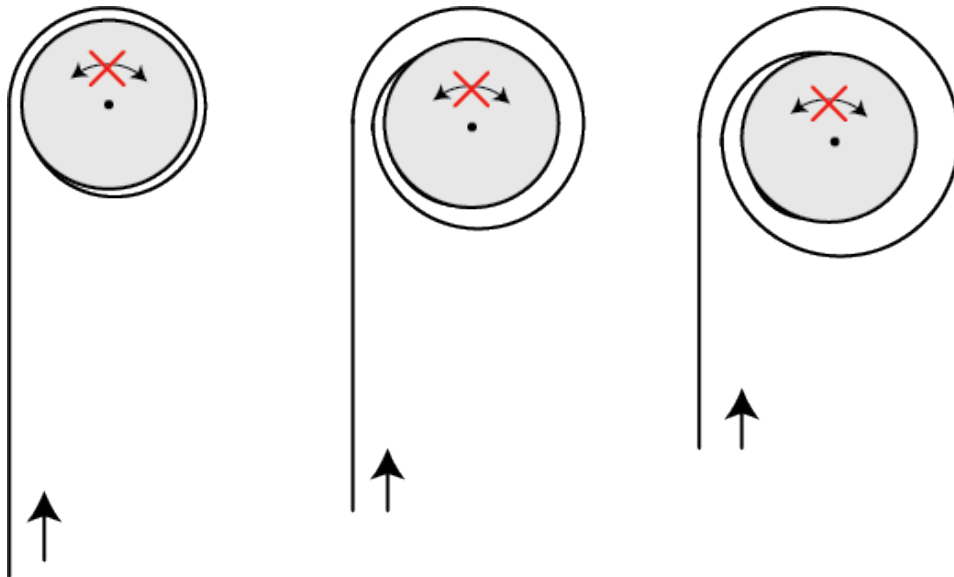


Figure 3.7: Visualisation of blossoming. If the drum is restricted from rotating while the STEM is compressed, the STEM will blossom away from the drum.

3.6. Guidance Rollers

When the rotary damper is engaged during stance phase, the drum is subjected to a torque counteracting free rotation of the drum. This causes the STEM to blossom away from the coiling drum, despite its natural tendency to clamp onto it.

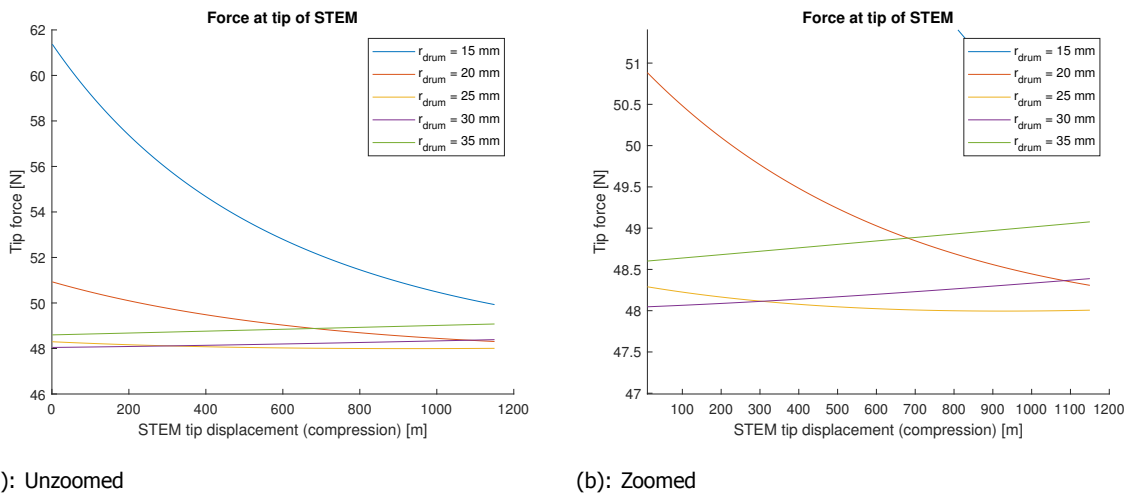


Figure 3.8: Force-displacement behaviour of coiling of a STEM for various drum radii. Force-displacement behaviour for drum radii upwards of 25mm remain near constant along the displacement range.

In order to constrain blossoming to a minimum, guidance rollers are placed around the STEM. While the damper is engaged, the STEM will blossom until it touches the guidance rollers. From this point on the load is transferred through the rotary damper. The guidance rollers are placed around the drum in a circular pattern with just sufficient space between the roller and drum, such that the STEM is able to coil up without jamming for kneeling and squatting. Based on the curve for a drum of radius of 25mm in Fig. 3.6, the room between the edges of the drum and guidance rollers is chosen to be 4mm. The guidance rollers are made of aluminium and have a radius of 5mm.

3.7. Balancing Spring

As described in Sec. 3.5, coiling a STEM induces elastic strains in the material, resulting in a spring-like behaviour of the STEM. It was also established that this behaviour is undesired due to the resisting force during retraction of the legs. Therefore it is advantageous to reduce or mitigate this force-displacement behaviour, shown in Fig. 3.8, through the use of a balancing spring.

Appendix. F shows how the spring was chosen. Similar to the force-displacement curve, the torque-rotation curve turned out to be fairly constant as well. Therefore a constant torque spring was chosen, i.e. a constant torque spring by Hunter Spring and Reel (product no. 20012) [20]. Its dimensions are shown in Table 3.2. Refer to Fig. 3.9 for an accompanying image clarifying the dimensions. The maximum residual force after balancing the spring behaviour of the STEM was 13N.

Due to availability and order issues with the manufacturer, it was decided to not use a balancing spring for the prototype. The balancing spring will still be considered for the theoretical concept. Assuming that the torque-rotation characteristic is as stated in Table 3.2, the final mechanism can still be validated.

3.8. Rotary Damper

The controllable rotary damper is the element that provides a supporting force during walking. It was decided to use the same damper as a previous version of the Exobuddy [21].

As stated in Sec. 2.1.4, the load should only be supported during the stance phase. This implies that a damping action is required during stance phase, and no damping action is required during swing phase, kneeling and squatting. The chosen damping mechanism consists of a gear pump, a electric clutch and a one way freewheeling bearing. It is established that extension of the STEM never requires support. The freewheeling bearing will decouples extension from the gear pump. Compression of the

Table 3.2: Dimensions of the chosen constant torque spring with product number 20012 from Hunter Spring and Reel.

Dimension	Value
Torque (Nm)	1.02
Storage drum D2 (mm)	38.86
Output drum D3 (mm)	67.82
Storage flange D1 (mm)	62.2
Output flange D4 (mm)	84.33
Centre to Centre S (mm)	84.33
Thickness T (mm)	0.3
Width W (mm)	19.05

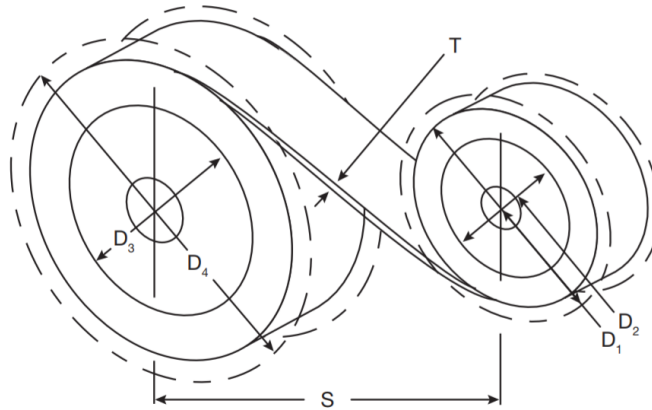


Figure 3.9: A schematic of a constant torque spring along with its relevant dimensions.

STEM on the other hand requires selective support or no support. The electric clutch allows compression of the STEM to be decoupled from the gear pump when no support is necessary and coupled to the gear pump when support is necessary.

3.9. Expected Performance

Each component has been dimensioned and the performance metrics are summarised in the table below. The desired values are also displayed. It can be seen that all the requirements are met.

Table 3.3: Requirements for assessment

Requirement	Desired Value	Expected Value
Support backpack load during walking	>300N	394N
Does not buckle	>300N	394N
Residual force at feet	<20N	13N
Lightweight	<14kg	6.06kg
Close to body (Max. dimensions)	<200x344x1150mm	140x319x1150mm
Distance between backpack and shoe	min. 300mm, max. 1150mm	min. 300mm, max. 1150mm

4

Evaluation

While the design may satisfy the requirements theoretically, it is important to also validate the performance in practice. To this end a prototype was built and tested, which is described in this chapter. First, the fabrication of the prototype is presented. Then the experimental setup and experiment are described and finally the results are presented.

4.1. Prototype

4.1.1. STEM

The STEM was fabricated from a glass fibre epoxy composite. A glass fibre sleeve was pulled over and secured to a PVC pipe, which served as the mould. Then the sleeve was impregnated with epoxy resin, after which a shrink sleeve was pulled over the pipe. Using a heat gun and shrinking the sleeve from one side to the other, excess resin was squeezed, resulting in a smooth homogenous surface. This was left to cure for two days. The shrink sleeve was then torn off and using a dremel, a long cut along the length of the pipe was made. Finally, approximately 5cm was cut off the ends to obtain clean, smooth edges. A picture of the resulting STEM is shown in Fig. 4.1. The properties of the fabricated STEM are given in Table 4.1. An elaborate description of the STEM fabrication procedure can be found in Appendix. G.

Property	Value
Inner radius (mm)	25
Thickness (mm)	0.75
N layers (-)	2
Length (mm)	1300
Fibre orientation angle (°)	60

Table 4.1: Properties of the fabricated STEM)



Figure 4.1: An image of the finished STEM

4.1.2. Side Plates

Two side plates were laser cut from an 8mm thick Plexiglas plate. Holes for a coiling drum, 12 guidance rollers and three spacer rods were also cut in the side plates. Additionally, an U-shaped hole was cut in each of the plates, such that a steel plate can be placed in between. This plate can then later be used to clamp the total system down for testing purposes.

4.1.3. Coiling Drum

The coiling drum is made of an aluminium rod, of which the ends are turned to a smaller radius to fit in between the side plates. Additionally, after turning, the coiling a shallow flat edge was milled on the drum. On this flat edge, a set of three holes was drilled and threaded, such that the STEM can be bolted onto this edge. By milling the edge, the bolt heads do not extend further than the radius of the drum, which would otherwise interfere with the coiling of the STEM onto the drum. This is visualised in Fig. 4.2. Additionally, a keyway is milled into the end of the drum. A key can then be used to fix the drum to the damper. On the other side of the drum, the same can be done for the connection to the balancing spring. The coiling drum is able to rotate freely with respect to the side plates. Lubricated, PTFE (Teflon) plain bearings are added at the rotating interface in order to reduce friction. The radius of the drum is 25mm. The width of the drum is 160mm, slightly larger than the width of the flattened STEM ($25 \cdot 2 \cdot \pi = 157\text{mm}$).

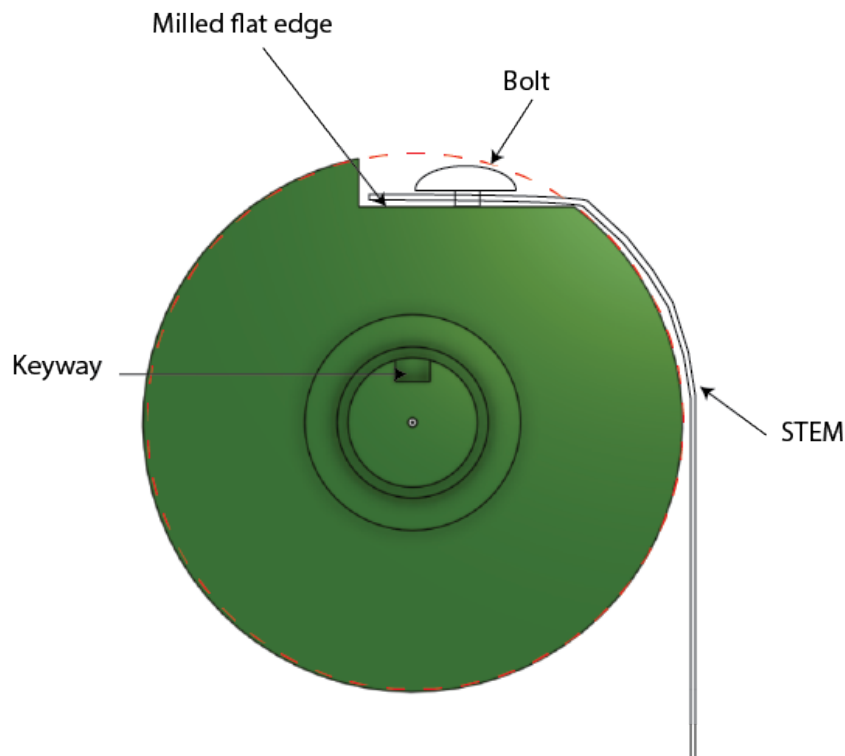


Figure 4.2: A side view of the coiling drum. The milled flat edge allows the bolt fastening the STEM onto the drum to stay flush with the STEM as it coils.

4.1.4. Guidance Rollers and Spacer Rods

A total of 12 guidance rollers and three spacer rods were hand turned from aluminium. The guidance rollers are able to rotate freely between the two side plates. In order to reduce the friction, lubricated, PTFE plain bearings were added at the rotating interface. The spacer rods merely act as spacers between the side plates, maintaining them at a fixed distance (170mm) from each other, so that the other components can fit in between.

Fig. 4.3 shows the containment mechanism, which is made up of the side plates, coiling drum, guidance rollers and spacer rods. Technical drawings of the turned and laser cut components can be found in Appendix. H.

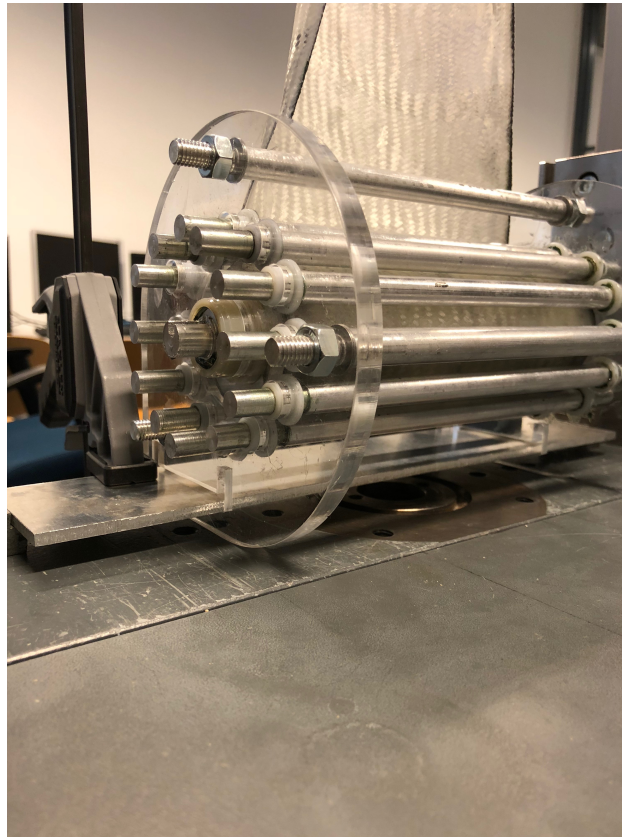


Figure 4.3: The containment mechanism

4.2. Experiments and Results

Three experiments have been conducted towards the assessment of the performance of the prototype, which will be described in this section. The first experiment is a test to find out at what load the STEM fails as a column, i.e. failure due to buckling. The second experiment is an extension to the first experiment and is a test to find out at what load the STEM fails as a result of the reduced bending stiffness of the STEM near the coiling drum. The third experiment is performed to find out what the maximum residual force is during free compression and extension of the STEM. All of the experiments are performed in a tensile tester by Zwick/Roell, model no. Z005.

4.2.1. Experiment 1

For the following experiment, the STEM is tested in its extended state, i.e., as a slit tube. The experiment is conducted to find out at what load the STEM fails purely due to buckling.

Setup

The setup is shown in Fig. 4.4. The ends of the STEM are constrained to remain in a tubular cross section. This is done by clamping the ends of the STEM onto an aluminium cylinder. The ends of the cylinders are subsequently connected to the tester through a spherical joint. The spherical joint is used in order to eliminate any eccentricity in the applied load. Fig. 4.5 shows the end conditions of the STEM. The STEM will be compressed until failure occurs. Due to the limited height of the tester, the full length of the STEM did not fit. The largest length fitting in the tester was 974mm. The constraining clamps each have a height of 40mm, therefore the effective length becomes $974 - 2 \cdot 40 = 894\text{mm}$. The STEM is compressed until failure occurs. This is repeated 5 times, after which the STEM is cut slightly shorter and the test is repeated. In total four different lengths are tested. For each length, the theoretical buckling force is calculated. The complete test setup is shown in Fig. 4.6.

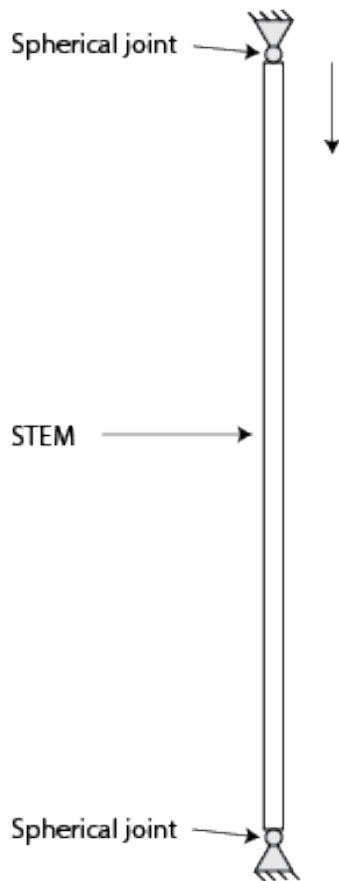


Figure 4.4: Setup for Experiment 1.



Figure 4.5: End conditions of the STEM for Experiment 1: the end of the STEM is constrained into a tubular shape and connected to the tensile tester through a spherical joint.

Results

The measurements for each of the four tested lengths are combined in box plots and presented in Fig. 4.7.

The recalculated critical buckling loads for the tested lengths, along with the mean measured buckling forces are presented in Table 4.2. It can be seen that as the length of the STEM decreases, the buckling

Table 4.2: Calculated and measured, average buckling forces, for various tested lengths of a STEM

Length	Calculated Buckling Force	Measured Buckling Force (mean)
894mm	653N	577N
847mm	728N	539N
800mm	816N	535N
720mm	1007N	552N

force remains the same or even decreases. It should be noted that during the tests, the same specimen was used over and over. Additionally, it was observed that each time buckling occurred, this took place at the same location, suggesting a local weak spot.



Figure 4.6: The complete test setup for Experiment 1

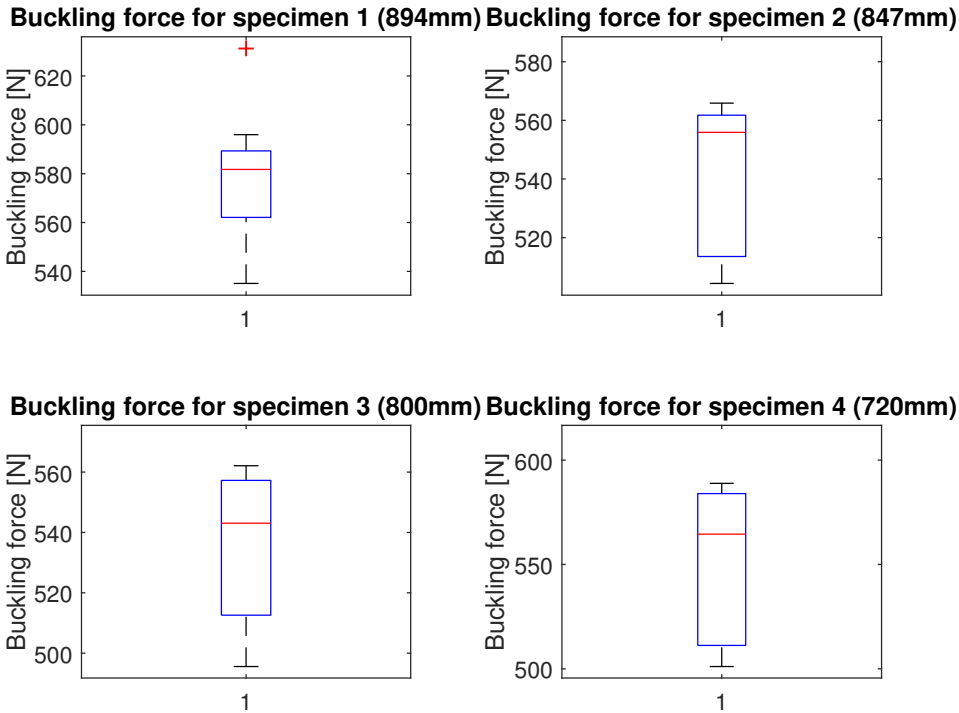


Figure 4.7: Measured buckling loads

4.2.2. Experiment 2

This experiment investigates the failure mechanism of the STEM while it is connected to the drum, i.e., a partially coiled STEM, and a load is being supported.

Setup

In this test, the STEM is fixed onto the drum and partially coiled. The containment mechanism is connected to the bottom of the tensile tester, whereas the free end is connected to the top of the tensile tester. This done to eliminate the effect of the weight of the containment mechanism. The drum is constrained such that it can not rotate under the influence of compression of the STEM. Similar to the previous test, the upper, free end is constrained into a tubular shape and connected to the tensile tester through a spherical joint. The containment mechanism at the bottom is centred between the tensile tester and given a fixed connection.

While the bottom boundary condition does not comply completely with reality (where a spherical joint connection is present), it give us insight on the failure mechanism of a partially coiled STEM. Ideally, a spherical joint connection at the lower connection would be preferred, however due to the eccentrically located centre of mass of the containment mechanism, a torque is generated. The combination of this torque and placement of the guidance rollers, results in bending of the STEM without any applied force from the tensile tester. In order to find out what the failure load is, due to a compressive force, the mechanism is clamped, such that no torques are applied to the STEM. The test setup for this experiment is shown in Fig. 4.8. The STEM is compressed until the force measured reaches a maximum of approximately 300N and starts decreasing.



Figure 4.8: Test setup for Experiment 2, here the drum is constrained and can not rotate. The top connection is spherical, whereas the bottom connection is fixed.

Results

The compression test was performed for two starting lengths of the STEM, namely, at 530mm and 615mm. The results are shown in Fig. 4.9. It is observed that regardless of starting length, failure occurs at the same force. Additionally, the failure location, which is situated close to the coiling drum, is the same for each compression test, shown in Fig. 4.10. It was also observed that the STEM initially blossoms away from the coiling drum. The outer most coil starts, after which the subsequent inner coils also blossom outward. During blossoming, the force necessary to compress further increases very

slightly, until all coils are completely blossomed and are touching the guidance rollers, at approximately 20mm travel. From this point on, the force spikes up until failure occurs.

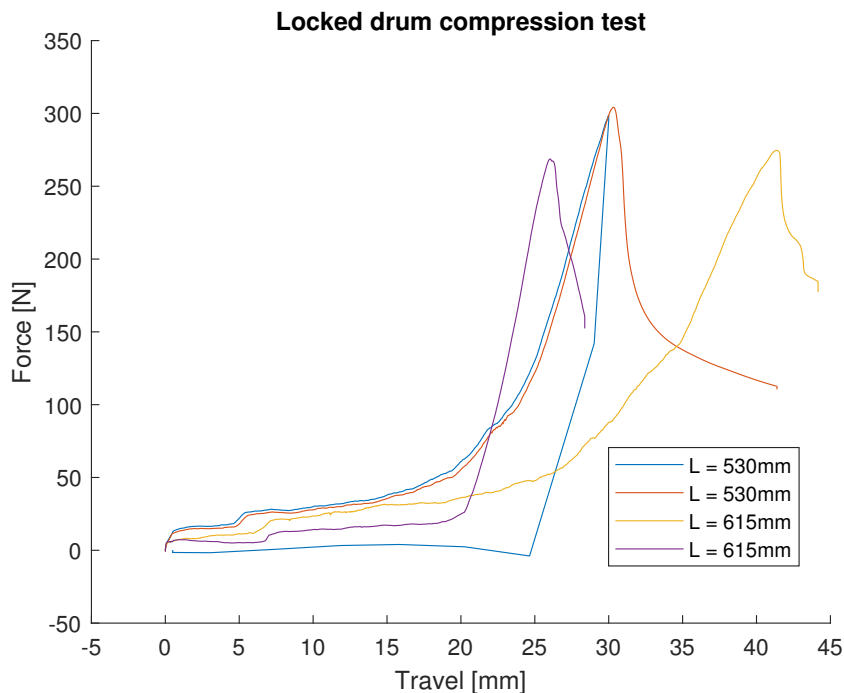


Figure 4.9: Results of Experiment 2. The STEM is compressed while the drum is restricted from rotating. The test was performed twice for two different starting lengths of the STEM.

4.2.3. Experiment 3

The following experiment is conducted to assess the force-displacement characteristic of the STEM during free compression and extension.

Setup

The setup for this experiment is identical to Experiment 2, however the rotational degree of freedom of the drum is not constrained. Three different travel distances are used, namely, 100mm, 200mm and 300mm. The STEM is compressed to a certain travel distance and then returned to zero travel. For each travel distance, the test is performed six times, amounting to a total of 18 tests.

Results

The results of the experiment are shown in Fig. 4.11. A hysteresis loop can be observed here. The top part of the curves corresponds to compression of the STEM, whereas the bottom part of the curves correspond to extension of the STEM. In other words, the loop was traversed in a clockwise fashion during the tests. Little spread between measurements is found and a slight increase in force is observed as the STEM is compressed more and more. As the travel nears 300mm, the force increases more dramatically. When comparing the measured characteristic to the calculated characteristic, shown in Fig. 4.12, it can be seen that the force-displacement curve of the measurement is less constant. However, for the majority of the travel, the measured force is lower than the calculated force. It should be noted that for neither of the two characteristics, a balancing spring is incorporated.

4.2.4. Prototype performance

The assessment criteria are consulted to assess the performance of the prototype. They are given in Table 4.3. All requirements are satisfied, except for the buckling requirement.



Figure 4.10: Failure during STEM compression takes form as a dent propagating in the material, after which the STEM continues to crumple and lose its load-bearing capacity.

Table 4.3: Assessment of Prototype

Requirement	Desired Value	Prototype Value
Support backpack load during walking	>300N	300N
Does not buckle	>300N	300N
Residual force at feet	<20N	<13N
Lightweight	<14kg	7.5kg
Close to body (Max. dimensions)	<200x344x1150mm	140x334x1150mm
Distance between backpack and shoe	min. 300mm, max. 1150mm	min. 300mm, max. 1150mm

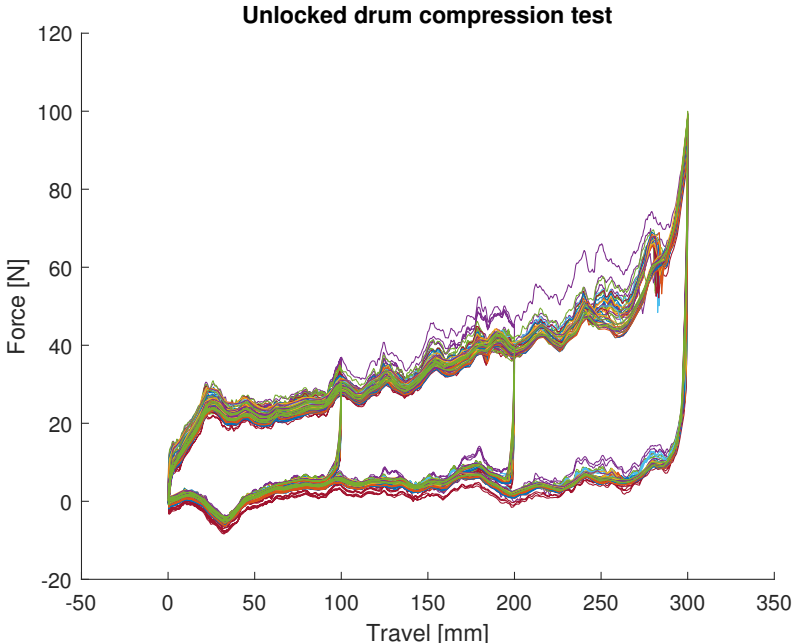


Figure 4.11: Results of Experiment 3. The STEM is compressed while the drum is free to rotate. Each test consisted of compression and extension of the STEM.

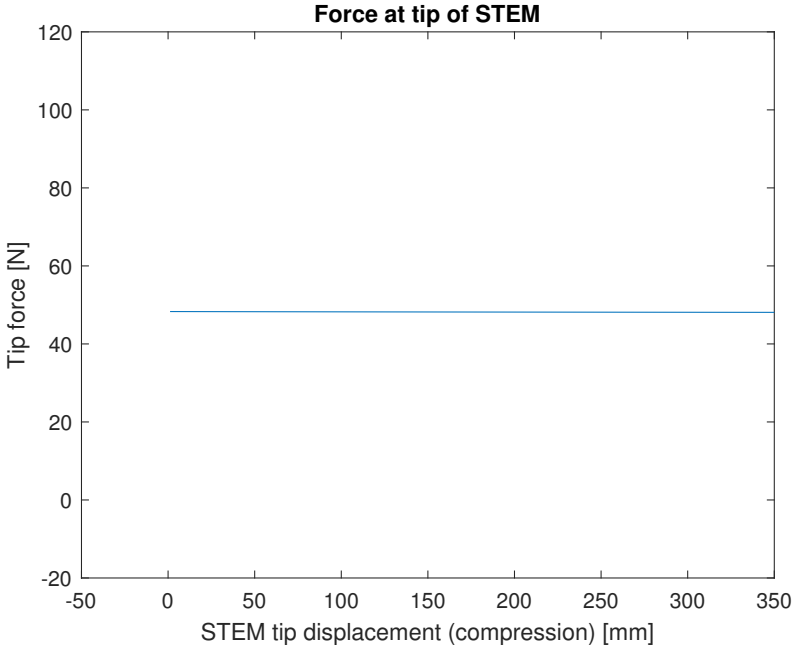


Figure 4.12: Theoretical force-displacement curve

5

Discussion

In this research, we set out to design a load-carrying exoskeleton with a small occupied space during operation. The selected concept was based on STEMs. In order to validate the proposed design, several tests were performed on a prototype.

Experiment 1

First, a buckling test was performed where the fabricated STEM was in its fully extended state. A compression test was performed on several different lengths of STEM. The results (presented in Table 4.2) showed that, contrary to Euler's buckling criterion, the critical force remained almost constant for decreasing lengths of the STEM. One would expect an increase in the critical force, as the length decreases. Buckling of the STEMs was assumed to be elastic and therefore tested STEMs were cut short and retested as a specimen with a different length. A possible explanation for the stagnating critical force could be that imperfections and damage done prior to buckling had created weak regions on the STEM. This explanation is further strengthened by the fact that each time buckling occurred, it occurred at the same location.

Experiment 2

Next, another compression test was conducted, however with a partially coiled STEM, instead of a fully extended STEM. The STEM was partially coiled onto a drum and the drum was constrained from rotating. It could be the STEM failed at the same location constantly. As the STEM nears its critical force, a dent starts to become visible near the flattened part of the STEM. The test was performed for different STEM radii and the critical force was similar for each test, suggesting that also here, a weak spot could have been present. Another fairly intuitive possible explanation is that near the drum, the STEM cross section is almost flat. The flat cross section has a much lower bending stiffness than the tubular shape, and therefore it can be expected that the STEM will fail near the drum first, regardless of imperfections in the material due to fabrication errors. While this critical force is fairly low, it is believed that by providing extra support at the location where the fold will occur, the critical force will increase. This suspicion arose after a couple of quick hand tests, where an additional guidance roller was placed at the folding location.

Experiment 3

A final test was conducted to obtain the force-displacement characteristic of the STEM during free rotation. Force is generated due to the storage of strain energy. A constant was predicted, whereas the measured curve had a slight increase as the STEM was compressed further. Near the end of the compression range, a more drastic increase in force could be seen. With any partially coiled STEM, a transition zone can be seen, which is the region in which the cross section is neither flat nor tubular, but something in between. It is thought that the transition zone is the source of the slight increase in force per unit compression, as it is influenced by the coiling of the STEM. The more the STEM coils,

the more the transition zone is affected and therefore the more drastic increase at the end. It was also clear that overall, the measured force was lower than the calculated force. A possible explanation of this is relaxation of the composite material. As the STEM is stored in its coiled configuration for a long time, it may slowly adopt that configuration as its lowest energy state, reducing the extension force. This phenomena could prove to be useful perhaps in the design of a statically balanced tape spring without external springs.

During this test it was also found that during free extension and compression of the STEM, the STEM was clamped always clamping onto the drum, suggesting that tailoring the natural coiling radius smaller than the transverse radius can result in a compact system and possibly eliminating a containment mechanism with guidance rollers. However for the current application this is not feasible due to the necessity of guidance rollers when the damper is engaged and a load is transferred.

Production

During the prototyping process, it was found that there is a limited assortment of fibre sleeves, limiting the freedom in tailoring the material properties of a laminate. Additionally, as composite products are often manually manufactured, human errors may become an issue

6

Conclusion

During this thesis the redesign of the mechanical structure of a load-carrying exoskeleton was performed. The proposed design was based on Storable Tubular Extendible Members (STEMs). STEMs possess the convenient property of having significant structural integrity in their extended state, but are easily coiled up into a compact roll. A device was designed, fabricated and assessed according to a set of criteria. We have shown that STEMs are a suitable candidate when it comes to the design of compact and lightweight load-carrying exoskeletons. By using fibre reinforced composites as the STEM material, it is possible to tailor the natural coiling radius of the STEM, allowing for the choice of smaller storage drums, contributing to more compact designs. It was found that while composite materials offer great tailor-ability of material properties, the fabrication procedure remains tricky and is quite sensitive to imperfections.

In comparison to conventional exoskeletons, STEM inspired exoskeletons are lightweight and can be stowed very compactly. Furthermore, due to the prismatic motion of the device, it is easily fitted to users of various sizes and lengths.

We have shown that the use of STEMs extends further than the aerospace industry alone.

6.1. Future work

An possible, interesting idea would be to omit the damper and balancing spring in a STEM based exoskeleton completely and exploit the spring behaviour of the compressed STEM. This spring behaviour could possibly be tailored to certain specifications by changing the laminate configuration of the fibre reinforced composite STEM. Doing this may result in a truly lightweight device.

While relaxation is often undesired, in a composite STEM, it may be used to balance a STEM without external components. This could possibly be done by fabricating the STEM in one configuration and stowing it in the other configuration.

In this work, the damping mechanism was adopted from old previous research. It may be worthwhile to invest in the research of other, more compact, damping mechanisms.

Durability and robustness were not considered during this research. Especially when applied to a product intended for military use, these factors should be considered.

Bibliography

- [1] M. Corps, *Marine Corps Planning Process*, (2010).
- [2] M. Holewijn, *De militaire bepakking, adviezen over het gewicht en de verdeling*, (1990).
- [3] J. Knapik, K. Reynolds, and E. Harman, *Soldier load carriage: historical, physiological, biomechanical, and medical aspects*, *Military medicine* **169**, 45 (2004).
- [4] *Introduction to Indego*, (2015).
- [5] *ReWalk 6.0 – Home*, .
- [6] *Ekso GT™ Robotic Exoskeleton Cleared by FDA for Use With Stroke and Spinal Cord Injury Patients :: Ekso Bionics Holdings, Inc. (EKSO)*, .
- [7] A. Zoss, H. Kazerooni, and A. Chu, *On the mechanical design of the Berkeley Lower Extremity Exoskeleton (BLEEX)*, in *2005 IEEE/RSJ International Conference on Intelligent Robots and Systems, IROS* (2005) pp. 3132–3139.
- [8] J. Pransky, *The Pransky interview: Russ Angold, Co-Founder and President of Ekso™ Labs, Industrial Robot: An International Journal* **41**, 329 (2014).
- [9] *Raytheon XOS 2 Exoskeleton, Second-Generation Robotics Suit*, .
- [10] G. Pahl and W. Beitz, *Engineering Design: A Systematic Approach, 3rd Edition* (2007).
- [11] G. Bovi, M. Rabuffetti, P. Mazzoleni, and M. Ferrarin, *A multiple-task gait analysis approach: Kinematic, kinetic and emg reference data for healthy young and adult subjects*, *Gait Posture* **33**, 6 (2011).
- [12] DINED, *Anthropometric database*, .
- [13] J. Ekelöv, *Design and manufacturing of thin composite tape springs*, (2014).
- [14] V. Lappas, N. Adeli, L. Visagie, J. Fernandez, T. Theodorou, W. Steyn, and M. Perren, *CubeSail: A low cost CubeSat based solar sail demonstration mission*, *Advances in Space Research* **48**, 1890 (2011).
- [15] K. A. Seffen and S. Pellegrino, *Deployment of a Rigid Panel by Tape-Springs Release*, , 355 (1997).
- [16] J. Costantine, Y. Tawk, C. G. Christodoulou, J. Banik, and S. Lane, *CubeSat Deployable Antenna Using Bistable Composite Tape-Springs*, **11**, 285 (2012).
- [17] O. Soykasap, S. Pellegrino, P. Howard, and M. Notter, *Tape Spring Large Deployable Antenna, 47th AIAA/ASME/ASCE/AHS/ASC Structures, Structural Dynamics, and Materials Conference 1-4 May 2006 Newport, Rhode Island*, 1 (2006).
- [18] F. P. J. Rimrott, *Two Secondary Effects in Bending of Slit Thin-Walled Tubes*, *Journal of Applied Mechanics* **33**, 75 (1966).
- [19] A. Hoskin, A. Viquerat, and G. S. Aglietti, *Tip force during blossoming of coiled deployable booms*, *International Journal of Solids and Structures* **118-119**, 1339 (2017).
- [20] H. Spring and Reel, *Constant torque spring catalog*, .
- [21] C. Koerhuis, F. Krause, and W. V. Dijk, *Exobuddy: een (semi-)passief exoskelet dat de last ondersteunt tijdens langdurige verplaatsingen*, (2017).

-
- [22] M. Ashby, *Materials: Engineering, Science, Processing and Design* (2013).
- [23] F. Rimrott and G. Fritzsche, *Fundamentals of STEM Mechanics*, , 321 (2000).
- [24] P. Mallick, *Fiber-reinforced Composites: Materials, Manufacturing and Design* (2007).
- [25] O. Soykasap, *Micromechanical Models for Bending Behavior of Woven Composites*, [Journal of Spacecraft and Rockets](#) **43**, 1093 (2006).
- [26] S. Timoshenko, *Theory of plates and shells* (1989).

A

Literature Review

Human gait & Lower limb exoskeletons for assistance and augmentation

Literature review

K.K.H. Lam

Technische Universiteit Delft

Human gait & Lower limb exoskeletons for assistance and augmentation

Literature review

by

K.K.H. Lam

Faculty of Mechanical, Materials and Maritime Engineering (3mE)

Contents

List of Tables	iii
List of Figures	iv
1 Introduction	1
1.1 Background	1
1.2 Research goal	1
1.3 Outline	1
2 Level ground gait	2
2.1 Biomechanics of human gait	2
2.1.1 Terminology and conventions	2
2.1.2 Gait analysis	4
2.1.3 Gait kinematics and kinetics	5
2.2 Effects of load carriage	7
2.2.1 Kinematics	7
2.2.2 Ground reaction forces	8
2.2.3 Metabolic cost	8
2.2.4 Health	8
2.2.5 Bodyweight unloading experiments	9
3 Lower limb exoskeletons for assistance and augmentation	10
3.1 Methods	10
3.1.1 Search method	10
3.1.2 Classification	10
3.1.3 Metrics	11
3.2 Results	11
3.3 Discussion	16
3.4 Conclusion	17
Bibliography	20

List of Tables

3.1	Sets of keywords used for the state-of-the-art search	11
3.2	Overview of exoskeletons found. Metrics annotated with (*) are approximated based on comparisons of their components with other similar exoskeletons. Metrics annotated with (-) could not be found or approximated properly. Metrics annotated with n/a were not applicable to the exoskeleton in question.	14

List of Figures

2.1	Human body with reference planes and directions (from [1])	3
2.2	A single gait cycle visualized (from [1])	5
2.3	Visualization of single and double leg support (from [1])	6
2.4	Joint angles, moments and powers in the sagittal plane (from [1])	6
2.5	"M"-shaped curve of vertical ground reaction forces during stance phase (from [2]) . .	7
2.6	Mean vertical and antero-posterior GRF (from [3])	8
3.1	Weight, load carrying capacity and load carrying capacity to weight ratio grouped according to number of actuated DoFs (a, c, e) and power source (b, d, f)	15
3.2	Images of reviewed exoskeletons	18
3.3	Images of reviewed exoskeletons (<i>continued</i>)	19

1

Introduction

1.1. Background

In the military, missions often require troops to carry heavy loads individually. Throughout history this load has only increased. In ancient times, extra equipment was often carried by auxiliary aids, such as horses and carts. As armies became more disciplined along the years, troops were required to depend less on auxiliary aids and carry the extra equipment by themselves. Missions that do not allow the use of wheeled vehicles also result in an increased backpack load for the soldier. Moreover, as technological advances introduce new specialized gear for soldiers, naturally, the amount of gear to carry with also increases. Previous studies indicated that load carriage not only contributes to acute and chronic injuries, but also adversely affects tactical performance [3–6].

Considering that the load required to be carried by military personnel is ever increasing, while the load carrying capacity of the human is not, there is the need to reduce the load on the user. Exoskeletons may very well fulfill this need. More specifically: load-carrying exoskeletons. [5]

An exoskeleton is a device worn externally by a user, designed to aid in some way. The exoskeleton can fulfill a wide range of roles. It can assist in rehabilitation therapy, assist impaired individuals in every day activities and even augment the user's capabilities.

1.2. Research goal

The goal of this study is to serve as a stepping stone towards the design of a quasi-passive lower limb exoskeleton for load carriage. The intended application is to aid foot soldiers during long marches where they have to carry heavy backpacks.

To this end, a study on level ground gait is done and a review on the state-of-the-art lower limb exoskeletons is conducted. The review will focus on assistive and augmentative lower limb exoskeletons. Load carrying exoskeletons, belonging to a class of augmentative exoskeletons are of particular interest to this research due to the necessity of such devices in the military.

1.3. Outline

This study consists of two chapters. In chapter 2, an analysis is done on the level ground gait of the human. First the terminology is explained, after which gait phases and the kinematics and kinetics that occur during the phases are elaborated on. Further, the effects of load carriage on the human are presented.

Next, in chapter 3 a review of the state-of-the-art lower limb exoskeletons for assistance and augmentation is conducted. In this review exoskeletons will be categorized according to several classification criteria. Next, metrics are determined and the exoskeletons are compared. Finally, conclusions are drawn and future directions of lower limb exoskeletons for assistance and augmentation is put forth.

2

Level ground gait

This chapter provides background information on the human gait and the effects of load carriage. Load carriage in this context is referred to as the carriage of a backpack. As the effect of load carriage is most prominent in a military setting where foot soldiers have to cover great distances, this chapter will have an emphasis on military load carriage. Section 2.1 touches the human gait on a kinematic and kinetic level and section 2.2 discusses the direct and indirect effects of (military) load carriage.

2.1. Biomechanics of human gait

This section covers the level ground walking gait on a kinematic and kinetic level. The analysis will primarily focus on motion in the plane that offers a side view of the human, called the sagittal plane. During walking, the majority of the motions and forces take place in the sagittal plane.

2.1.1. Terminology and conventions

Before analyzing the gait, it is necessary to understand the terminology and conventions used in gait analysis. These will be treated in this section. The terms and conventions described next apply to an upright standing human body with both arms by the sides of the body and the palms facing forward. This particular position is called the *standard anatomical position*.

Reference planes

Three reference planes are used to describe the motion of the limbs:

- The sagittal plane: a plane that divides the human body from head to toe in left and right portions
- The coronal or frontal plane: a plane that divides the human body from head to toe in front and back portions
- The transverse plane: a plane that divides the human body in upper and lower portions

Relationship between body parts

There are six directional terms used to describe the position of body parts relative to each other. They are given below, accompanied by an example describing the position of a body part relative to the centre of the body [1].

- Anterior: in front of. The belly button is anterior to the centre of the body
- Posterior: behind. The buttocks are posterior to the centre of the body
- Superior: above. The head is superior to the centre of the body
- Inferior: below. The feet are inferior to the centre of the body
- Left: self-explanatory

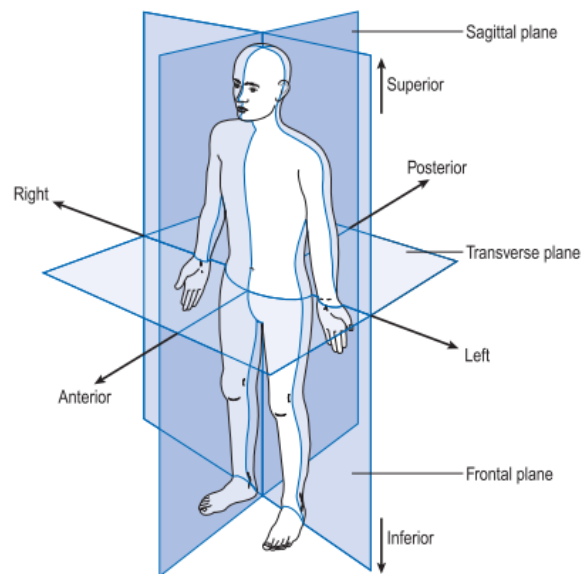


Figure 2.1: Human body with reference planes and directions (from [1])

- Right: self-explanatory

Figure 2.1 shows the standard anatomical position of the human, including reference planes and directional terms.

Additional terms can be used to describe directions within a body part. For this, it is helpful to define the *midline* of the body, which is an imaginary, vertical line going through the center of the body.

- Medial: towards the midline of the body. The big toe is on the medial side of the foot.
- Lateral: away from the midline of the body. The little toe is on the lateral side of the foot.
- Proximal: towards the rest of the body. The thigh is proximal to the shank, which is proximal to the ankle, which is proximal to the foot
- Distal: away from the rest of the body. The fingers are distal to the wrist, which is distal to the elbow, which is distal to the shoulder

Joint motion

The limbs move as a result of the rotation of the joints. The joint rotations are named differently depending on the plane in which they act, as well as the direction. The rotations are explained below, however without notion of rotational direction, as the conventions may vary per joint. The lower limb joints can be modeled in numerous ways depending on the use of the model. [7]. Here, the following simplification has been made for the lower limb joints: The hip is a three DoF joint, the knee is a one DoF joint and the ankle is a three DoF joint.

- Flexion and extension: rotation in the sagittal plane. For the ankle joint, these are called dorsiflexion and plantarflexion.
- Abduction and adduction: rotation moving a body part away or towards from the centre of the body.
- Internal and external rotation: rotation in the transverse plane.
- Inversion and eversion: rotation of the foot in the coronal plane.

The hip joint is able to rotate in each of the three reference planes. Hip flexion and extension are the rotations of the hip in the sagittal plane, that move the leg toward the front side and the backside of the body, respectively. The hip flexion/extension angle can be defined in two ways: by the angle between the vertical and the femur or by the angle between the pelvis and the femur. The latter is called the 'true' hip angle. Both definitions are used in gait analysis. Hip abduction and adduction are the rotations of the hip in the coronal plane, that move the leg away and towards the midline of the body. The hip abduction/adduction angle is defined by the angle between the femur and the vertical. Hip internal and external rotation are motions in the transverse plane that rotate the leg towards and away from the midline of the body, respectively. The hip internal/external rotation angle is defined with respect to the standard anatomical position, with the feet facing forward.

The knee joint is only able to rotate in the sagittal plane. Knee flexion and extension are the rotations of the knee that move the shank towards the backside and front side of the body, respectively. The knee flexion/extension angle is defined by the angle between the femur and the tibia.

The ankle joint is able to rotate in each of the three reference planes. Dorsiflexion and plantarflexion are rotations in the sagittal plane that move the foot towards the shank and away from the shank, respectively. The ankle dorsiflexion/plantarflexion angle is defined by the angle between the tibia and the foot. Although in a neutral position, this angle is around 90° , it is considered to be the 0° reference. Inversion and eversion of the ankle are rotations in the coronal plane, causing the soles of the feet to face inwards and outwards, respectively. The inversion/eversion angle is defined with respect to the standard anatomical position, where the feet are oriented flat.

Abduction and adduction of the ankle are rotations in the transverse plane, causing the toes to point outwards and inwards, respectively. The abduction/adduction angle is defined with respect to the standard anatomical position, where the feet are oriented forward.

2.1.2. Gait analysis

Human gait is a cyclic pattern of movement that is repeated step after step. Due to the cyclic nature of gait, it can be described by a single cycle of one leg. Although any instance in the gait cycle can be chosen to be the start and end, the following convention is used: the gait cycle starts when one foot first makes contact with the ground and ends when the same foot makes contact with the ground again [1, 8]. The gait cycle can be partitioned into phases in a number of ways, ranging from two phases to eight phases [9]. The partitioning as described by [1] is elaborated on in this section.

Events

During the gait cycle of a single leg, seven events occur, dividing the gait cycle into seven phases. The events that occur are:

- Initial contact: The foot touches the ground
- Opposite toe off: The foot of the opposite leg loses contact with the ground
- Heel rise: The heel of the foot loses contact with the ground
- Opposite initial contact: The foot of the opposite leg touches the ground
- Toe off: The foot loses contact with the ground
- Feet adjacent: Both feet are adjacent to each other
- Tibia vertical: The tibia (shank bone) is oriented vertically

Phases

Viewed in a simple manner, the gait cycle consists of two phases: the stance phase and the swing phase. The stance and swing phase of the gait cycle take up approximately 60% and 40% of the gait cycle, respectively. Viewed in a slightly more elaborate fashion, the gait cycle consists of seven phases, the first four of which take place during the stance phase and latter three take place during the swing phase [1]. The seven phases that make up the gait cycle are:

1. Loading response: Initial contact commences this phase. This phase lasts from 0 to 10% of the gait cycle.

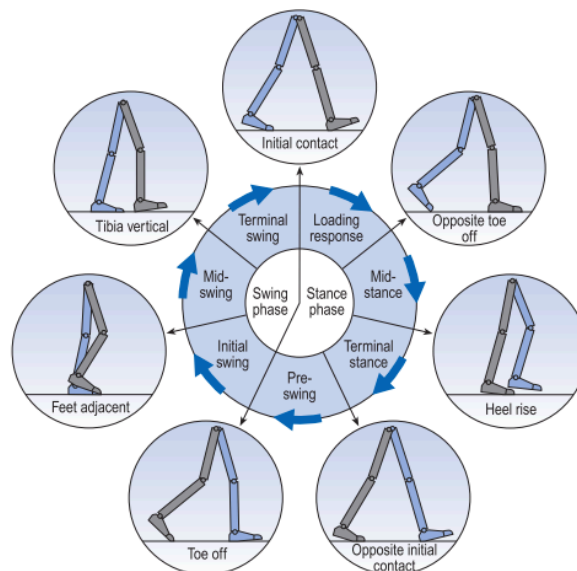


Figure 2.2: A single gait cycle visualized (from [1])

2. Mid stance: Opposite toe off commences this phase. This phase lasts from 10 to 30% of the gait cycle.
3. Terminal stance: Heel rise commences this phase. This phase lasts from 30 to 50% of the gait cycle.
4. Pre-swing: Opposite initial contact commences this phase. This phase lasts from 50 to 60% of the gait cycle.
5. Initial swing: Toe off commences this phase. This phase lasts from 60 to 70% of the gait cycle.
6. Mid-swing: Feet adjacent commences this phase. This phase lasts from 70 to 85% of the gait cycle.
7. Terminal swing: Tibia vertical commences this phase. This phase lasts from 85 to 100% of the gait cycle.

Figure 2.2 shows the gait cycle accompanied by the phases and events that occur.

Walking and running

Walking gait is characterized by alternating periods of double-leg support and single-leg support. Double-leg support is a relatively short period where the stance phase of one leg starts before the end of the stance phase of the other leg, introducing an overlap in the stance phases of both legs. During this period both legs provide support and the weight is transferred from one leg onto the other. Single-leg support is the period where only a single leg is in contact with the ground. Generally, the double stance period takes up approximately 10% of the gait cycle. Figure 2.3 shows a little more than a single gait cycle for both legs, illustrating the single-leg and double-leg support phases and their occurrences in time. In addition to single-leg and double-leg support another period can be identified: double-leg flight. This is when both legs are no longer in contact with the ground. When the gait cycle characterizes itself with alternating periods of single-leg support and double-leg flight, it is considered a running gait. Therefore a clear distinction between running and walking can be made: walking is characterized by having at least one leg in contact with the ground at all times, whereas running is characterized by having periods of no limb contact during the gait cycle [10].

2.1.3. Gait kinematics and kinetics

During walking gait, muscles near joints contract to generate torques about them in order to move the adjacent limbs. This section will treat the kinematics and kinetics of gait at the joint level.

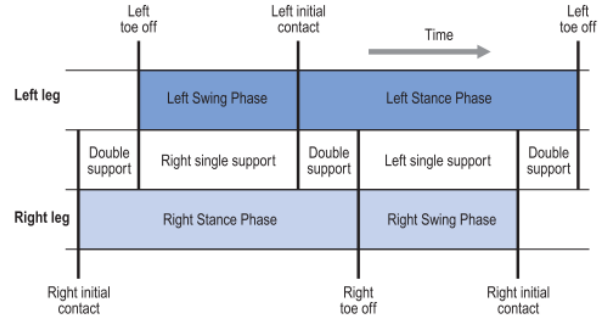
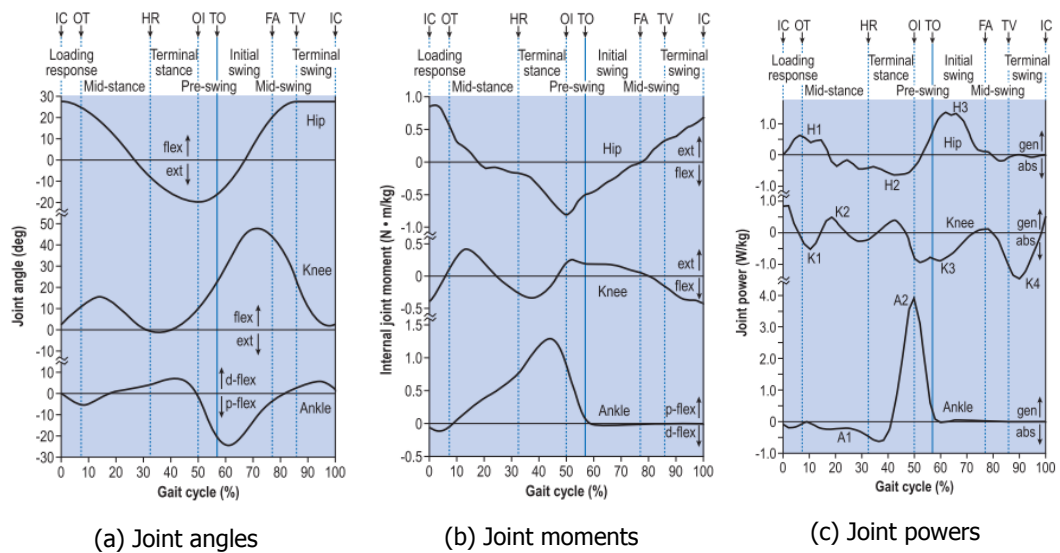


Figure 2.3: Visualization of single and double leg support (from [1])



(a) Joint angles

(b) Joint moments

(c) Joint powers

Figure 2.4: Joint angles, moments and powers in the sagittal plane (from [1])

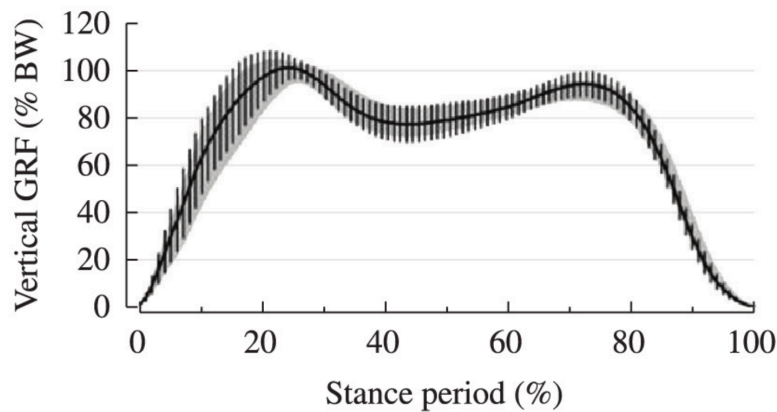


Figure 2.5: "M"-shaped curve of vertical ground reaction forces during stance phase (from [2])

Figures 2.4a, 2.4b and 2.4c show the joint angles, moments and powers in the sagittal plane during a single gait cycle for a 22 year old female of 55kg [1]. Though the exact values may not reflect the average of society, the course of the graphs does give a general view of the gait kinematics and kinetics of an individual. The figures will be used to elaborate on the kinematics and kinetics of the gait cycle.

Kinematics

Throughout the gait cycle, the hip joint transitions from a flexed position ($\approx 26^\circ$), to an extended position ($\approx -20^\circ$), back to a flexed position as it swings the leg back and forth once. The knee joint flexes twice during the gait cycle: once during the stance phase (to $\approx 15^\circ$) and once during the swing phase (to $\approx 48^\circ$). Flexion during the stance phase is necessary for the absorption of energy and flexion during the swing phase is necessary to clear the limb from the ground. The ankle joint plantarflexes (to $\approx -5^\circ$) during the loading response as the foot is placed flat on the ground. Then throughout mid stance, the ankle joint dorsiflexes (to $\approx 5^\circ$) until pre-swing, after which the ankle plantarflexes (to $\approx -25^\circ$) for push off into the swing phase. During the swing phase the ankle dorsiflexes in order to clear the ground [1, 10].

Kinetics

Unlike kinematics, kinetics (joint moments and powers) are not easily obtained from visual measurements. Generally, kinematics and ground reaction forces (GRFs) are combined with the help of inverse dynamics to calculate joint moments and powers [10]. GRFs are typically measured using force-plates or pressure sensors in shoes. The vertical GRF curve has a characteristic "M"-shape (see Figure 2.5), where two peaks can be identified. The first peak occurs during the loading response and the second peak occurs near the end of the pre-swing phase [2, 9, 11]. Muscles can do negative (absorptive) and positive (generative) work on joints. Negative work is done when a motion is slowed down, whereas positive work is done when motion is generated. In other words: negative work occurs when the direction of the muscle force is opposite to the direction of the motion and positive work occurs when the direction of the muscle force is in the same direction as the motion [12]. [13] conducted experiments on joint moment and energy patterns in normal gait and made some generalized observations: during the loading response, negative work is done by the knee joint, absorbing energy. During push off and toe off, the ankle and hip joints are the major contributors of positive work.

[12] conducted experiments on the distribution of positive and negative work in human gait. It was concluded that net muscle work is generally positive for level gait.

2.2. Effects of load carriage

Load carriage can have a number of effects on the human. They are elaborated on in this section.

2.2.1. Kinematics

[14] conducted experiments on the effect of military load carriage on the kinematics of gait. A variety of load carrying scenarios were imposed on the subjects, including walking with different guns and

loaded backpacks. It was found that a backpack load increased the forward inclination of the trunk in an effort to counteract the shift in center of mass. Furthermore an increase in walking speed was observed under influence of a backpack load compared to no load conditions. [15] conducted a similar experiment, however focused on pelvic movement. Increasing backpack loads led to minor increases in pelvic tilt and significant decrease in pelvic rotation. In order to facilitate greater shock absorption due to increased load, knee flexion after initial contact increases [16]. Double support phase duration is also increased as a result of increasing load [16, 17].

2.2.2. Ground reaction forces

Studies have been conducted on the effect of load carriage on ground reaction forces. Ground reaction forces are measured in three directions: medio-lateral, antero-posterior and vertical, with vertical being the most studied direction in gait, as the majority of the ground reaction force is in this direction. Unsurprisingly increasing load, results in increased ground reaction forces [3, 16]. Results from [3] show a fairly linear relationships between vertical and antero-posterior ground reaction forces and the carried load as can be seen in Figure 2.6, where the vertical and antero-posterior GRF, normalized to body mass, are displayed.

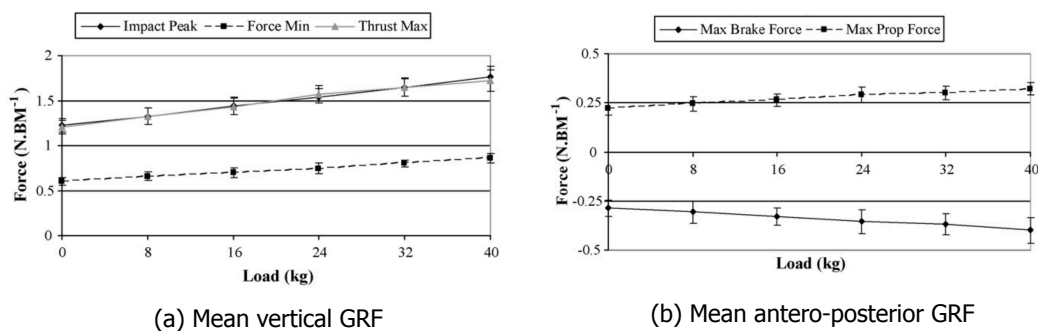


Figure 2.6: Mean vertical and antero-posterior GRF (from [3])

2.2.3. Metabolic cost

Walking, as any other activity of the human body requiring muscle contraction is associated with energy expenditure, also known as metabolic cost. [18] developed an empirical equation for the prediction of metabolic costs of walking. Beside body weight, walking speed, surface slope and terrain factor, the carried load was also a parameter in this equation. Due to the limitation of the equation only being applicable to walking speeds greater than 2.5km/hr, another study was conducted in an effort to revise the equation for the whole range of walking speeds showing a near linear relationship between carried load and metabolic rate [19]. [20] also reported a linear increase in metabolic rate as a function of carried load and furthermore concluded that the majority of the metabolic cost of walking can be attributed to the muscles doing work during the stance phase, indicating that the work of leg swing is relatively small during walking gait.

2.2.4. Health

The aforementioned effects of load carriage each contribute in one way or another to health issues and a decrease in cognitive capabilities.

The most common acute injury as a result of load carriage is foot blisters. They form due to the increased frictional forces between the socks and the skin. As the trunk leans more forward due to the load, more strain is exerted on the back muscles and spine resulting in lower back pain [4]. Other injuries have also been reported by [5]: stress fractures, knee pain, fatigue and "rucksack palsy". Rucksack palsy, otherwise known as "brachial plexus injury" can be identified by numbness or paralysis of the upper body. This occurs due to the shoulder straps compressing the nerves and damaging them [21].

Next to health issues, load carriage also decreases cognitive capabilities. Studies have shown that alertness diminished significantly under the influence of load carriage. [22] showed that during 20 km long marches, the mental alertness decreased with increasing carried load. [23] also found a decreased

alertness when walking with a 40 kg load. Especially visual and tactile cues were poorly recognized compared to auditory cues.

2.2.5. Bodyweight unloading experiments

[2] and [24] took different approaches to the matter of load carriage. [2] conducted body unloading experiments where a body weight support systems was applied to subjects. Respectively, 0%, 15% and 30% body weight support were applied and subjects ground reaction forces were measured on a force plate. It was found that with increasing body weight support, walking speed decreased and the characteristic "M"-shaped curve of vertical ground reaction forces flattened out. [24] conducted a similar research focusing on kinematics. Results indicated that kinematics showed minimal alterations, even at high levels of unloading (up to 50%). Temporal parameters, however showed some alterations: as body unloading increased, the duration of the double support phase decreased, being well in line with the results of [16] and [17] where increased load results in increased double support phase.

3

Lower limb exoskeletons for assistance and augmentation

An overview of the state-of-the-art lower limb exoskeletons intended for assistance and augmentation is presented in this chapter. This review investigates the kinematic architecture, actuation method, degrees of freedom and the performance of each exoskeleton. The terms *exoskeleton*, *wearable robot*, and *orthosis* are often used interchangeably in literature to describe an externally worn device that in some way aids the wearer [25, 26]. Generally, exoskeletons are associated with anthropomorphic devices that augment the user, orthoses are associated with devices that aid users with a limb pathology and wearable robots are associated with powered devices [27]. For the purpose of this review, we will use the term exoskeletons, even though non-anthropomorphic architectures are also considered.

3.1. Methods

3.1.1. Search method

In order to avoid investigating exoskeletons that are not relevant to the challenge introduced in Chapter 1, some restrictions have been imposed on the scope of the review. Only lower limb exoskeletons are considered. In the case of full body exoskeletons, only the lower limb part will be investigated. Devices that act on merely a portion of the lower limbs, such as ankle orthoses are not considered. Furthermore only portable devices are of interest. This means that devices tethered or connected to an auxiliary stationary point are not considered.

For this search, four sets of keywords were used on Scopus and Espacenet, shown in Table 3.1. The sets are combined using AND operators and the keywords within each set are separated by OR operators. A search on Google was also performed to find commercially available exoskeletons. In the case that no research documents that matched with the commercially available exoskeletons were found, technical data from their commercial site was gathered.

3.1.2. Classification

Several classification criteria can be established in order to compare the exoskeletons with one another. We have the following classification criteria:

Architecture Is the device anthropomorphic or non-anthropomorphic? In practice, exoskeletons are generally never truly anthropomorphic due to the complexity of the human joints. For example, the human knee joint is a rolling and sliding joint [28]. Here, we will consider devices that have their joints collocated with the human in the sagittal plane to be anthropomorphic.

Power source Is the device active, quasi-passive or passive? Passive devices do not require an auxiliary power source (such as a battery) to power their actuators, while active devices do. Devices using requiring power for a control system are considered quasi-passive, as long as the actuation itself does not consume power.

Table 3.1: Sets of keywords used for the state-of-the-art search

Sets	Keywords
Exoskeleton	exoskeleton ortho* wearable device wearable robot
Lower limbs	lower limb* lower extremity* lower body leg*
Assisting	load carr* weight carr* load support* load carr* assist* augment* enhanc*

Application What is the intended goal of the device? We identify three applications for the exoskeletons found: load carriage, increasing joint performance and aiding the impaired. Load carriage refers to the supporting role that the exoskeleton fulfills by supporting either body weight or an external load (i.e. a backpack). An exoskeleton is considered to increase joint performance if it brings about a metabolic cost reduction or increases the power of a joint by applying extra torques. If the exoskeleton gives function back to less-abled individuals, such as aiding in walking, sitting and standing up, we place it in the category of aiding the impaired. It is possible that an exoskeleton accomplishes multiple goals.

3.1.3. Metrics

Next, we use a number of metrics to evaluate the exoskeletons.

- Actuator type. We investigate in which way the exoskeleton is actuated.
- Weight. The total weight of the exoskeleton is determined.
- DoF. We determine the total number of DoFs per exoskeleton leg in order to assess the mobility of the device.
- Actuated DoF. The number of actuated DoFs per exoskeleton leg is analyzed.

The data found is summed up and different classes of exoskeletons are compared according to the metrics. In addition to the above stated metrics, for load carrying exoskeletons, we also investigate the load carrying capacity.

3.2. Results

This section presents the results of the literature review. A total of 60 exoskeletons was found. Through filtering the devices out that were not in the scope as outlined in section 3.1.1, we were able to reduce the number of exoskeletons down to 26.

The majority (19 out of 26) of the exoskeletons found had an anthropomorphic architecture. The exoskeletons form parallel leg structures on the lateral sides of the human legs. Such devices tend to mimic the kinematics and thus also the working principle of the human limbs by applying torques at the joints. In order to apply torques and maintain alignment with the human legs, thigh and shank braces are used. The use of braces varies from both thigh and shank braces [29–36] to only thigh braces [37–45] to no braces at all.

A small number (7 out of 26) of non-anthropomorphic exoskeletons was found. NAEIES [46], ExoBuddy

[47] and OLAD [48] contain ankle, knee and hip joints, however they are not collocated with the human joints. SJTU-EX [49] has its hip and ankle joints aligned with the human, however no knee joint is present. Instead, a scissor-like mechanism is used between the hip and ankle, acting as a prismatic joint to facilitate knee bending of the human. OX [50] is a non rigid exoskeleton comprising of two bowden cables running along the legs to the backpack. MoonWalker [51] provides support by means of a rigid link connecting a backpack and the shoe. With optimal ergonomics and dynamical properties in mind, using a novel approach in kinematic synthesis, the LENAR [31] was developed. The architecture is set up in a way such that it is insensitive to alignment accuracy and forces are transmitted orthogonal to body segments in order to avoid shear forces.

The found exoskeletons comprised mostly active ones (18 out of 26). Generally, batteries incorporated in a backpack-like harness provide the power. BLEEX [52] and XOS 2 [53] include a combustion engine in addition to batteries, due to their high power demands. BLEEX requires 1.143 kW of hydraulic power in order to carry a 75 kg payload, while walking at 1.3 m/s [52]. Next to actuators, a control system also has to be powered, generally requiring little power compared to actuation power.

Four exoskeletons were found to be quasi-passive, meaning they only require power for a control system. This control system regulates the activation and deactivation of passive elements that provide assistive or supportive forces [39, 47, 48, 51].

Finally, three exoskeletons were completely passive. XPED [32] uses a spring spanning over the hip, knee and ankle joints in an attempt to simulate artificial tendons which store and release elastic energy during walking. Both OX [50] and UPRISE [34] do not use elastic elements. OX transfers loads through bowden cables to the ground. UPRISE seemingly relies on proper alignment of the exoskeleton joints to transfer loads to the ground.

The largest part of the reviewed exoskeletons is intended for load carrying purposes. They are designed to carry heavy backpack loads, often in a military setting [34, 38–41, 43, 46–52].

Exoskeletons increasing joint performance either apply assistive torques to the wearer or attempt to increase efficiency of movement. The Agri-Robot [29] is designed to help agricultural workers in harvesting crops by applying assistive torques to the user. XPED [32] uses a single spring per leg in an attempt to reduce metabolic cost of walking by storing and releasing elastic energy at the right moments during the gait cycle.

The CUHK-EXO [37] is intended to assist paralyzed individuals in walking, sitting and standing up. Similar to Indego [33] and ReWalk [36], CUHK-EXO also includes a pair of crutches.

Some exoskeletons are reported to fulfill multiple purposes [30, 44, 45, 53, 54]. HAL-5 LB Type C [30] intends to aid spinal cord injury (SCI) patients in standing up and walking by taking over some of the work to be performed by the human joints. It also provides assistive torques and has body weight bearing capacities. HEXAR [54] and NTU [45] are designed to carry backpack loads can apply assistive torques as well due to the presence of active components at the joints.

Electric motors and hydraulic cylinders are the most prominent actuator types. A total of 13 and 8 uses were seen for electric motors and hydraulic cylinders, respectively. Electric motors are exclusively used in active exoskeletons, whereas hydraulic cylinders are used in both active and quasi-passive exoskeletons. In the active setting, hydraulic cylinders are powered and are generally double acting. In quasi-passive exoskeletons, hydraulic cylinders serve as damping mechanisms [39, 47, 49]. As such, they are not able to increase joint efficiency due to the lack of energy storage capabilities and are only used for load carrying applications.

The remaining types of actuation types are tension springs, gas springs, force balancers, magnetorheological dampers, bowden cables and alignment of the joints. The latter two [34, 50] do not provide energy storing or dissipative capabilities, but rather act as structural elements in order to transmit forces to the ground.

The weights of the exoskeletons varied from 3.86 kg to 95 kg.

The number of DoFs of the exoskeletons range from 3 to 7. Hip flexion/extension, knee flexion/extension and ankle dorsiflexion/plantarflexion are always allowed. Exoskeletons with seven DoF attempt to mimic the user's lower limb kinematically, by adopting the same DoFs. Generally, the rotation axes for hip adduction/abduction, hip rotation, ankle rotation and ankle adduction/abduction are not aligned

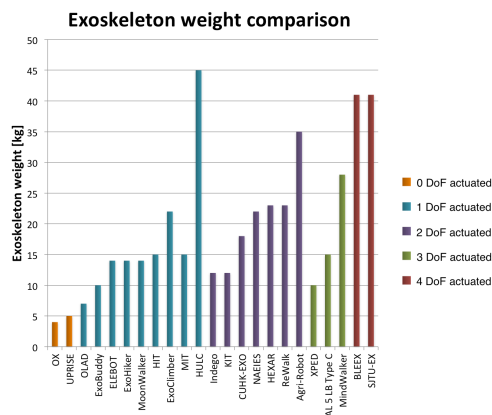
between exoskeleton and wearer.

The exoskeletons usually only actuate a portion of the total DoFs. Often a combination of actuated hip flexion/extension, knee flexion/extension and ankle dorsiflexion/plantarflexion is chosen due to the large metabolic power consumption relative to other DoFs [55]. In some cases, hip adduction/abduction is also actuated as it is deemed important for balanced walking [52].

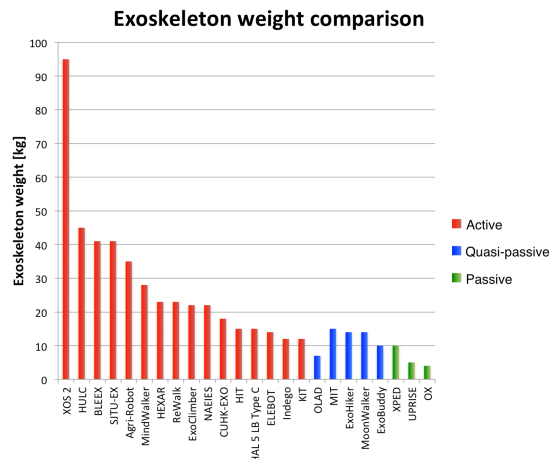
An overview of the exoskeletons along with their metrics is shown in Table 3.2. Figure 3.1 presents a comparison of the evaluated exoskeletons grouped by number of actuated DoF and power source. Weight, load carrying capacity and the load carrying capacity to weight ratio are shown. Furthermore, Figures 3.2 and 3.3 show images of the reviewed exoskeletons in order of appearance in Table 3.2.

Table 3.2: Overview of exoskeletons found. Metrics annotated with (*) are approximated based on comparisons of their components with other similar exoskeletons. Metrics annotated with (-) could not be found or approximated properly. Metrics annotated with n/a were not applicable to the exoskeleton in question.

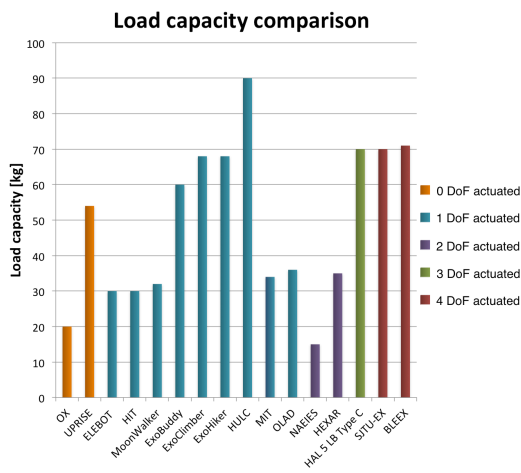
Architecture	Power source	Device	Load carriage	Increase joint performance		Actuator type	Weight [kg]	DoF per leg	Actuated DoF per leg		
					Aid impaired						
Anthropomorphic	Active	Agri-Robot [29]		✓		Electric motors	35	3	2		
		BLEEX [28, 56, 57]	✓			Hydraulic cylinders	41	7	4		
		CUHK-EXO [37]			✓		Electric motors	18	6	2	
		ELEBOT [38]	✓				Hydraulic cylinders	14*	7	1	
		ExoClimber [40]	✓				Hydraulic cylinders	22	7	1	
		HAL-5 LB Type C [30, 58, 59]	✓	✓	✓		Electric motors	15	7	3	
		HEXAR [42, 54]	✓	✓			Electric motors	23	7	2	
		HULC [41]	✓				Hydraulic cylinders	45	7	1	
		HIT [43]	✓				Electric motors	30	7	1	
		Indego [33, 60, 61]			✓		Electric motors	12	3	2	
	Quasi-passive	KIT [44]		✓	✓		Hydraulic cylinders	3.86	3	2	
		MINDWALKER [35]			✓		Electric motors	28	6	3	
		NTU [45]	✓	✓			Electric motors	41*	4	3	
		ReWalk [36, 62]			✓		Electric motors	23	7	2	
		XOS 2 [53]	✓	✓			Electric motors	95	-	-	
		ExoHiker [39]		✓			Hydraulic cylinders	14	7	1	
		MIT exoskeleton [63, 64]		✓			Magnetorheological dampers	15	7	1	
		Passive	XPED [32, 65, 66]			✓		Springs	10	4	3
			UPRISE [34, 67, 68]	✓				Alignment	5*	5	0
		Non-Anthropomorphic	Active	LENAR [31]			✓	Electric motors	-	4	2
NAEIES [46]	✓					Electric motors & Gas springs	22*	6	2		
SJTU-EX [49, 69]	✓					Electric motors & Hydraulic cylinders	41*	6	4		
Quasi-passive	MoonWalker [51]			✓			Gravity balancer	14*	7	1	
	ExoBuddy [47]			✓			Hydraulic cylinder	10	7	1	
	OLAD [48]			✓			Springs	7	3	1	
	Passive		OX [50, 70]		✓			Bowden cables	8	n/a	n/a



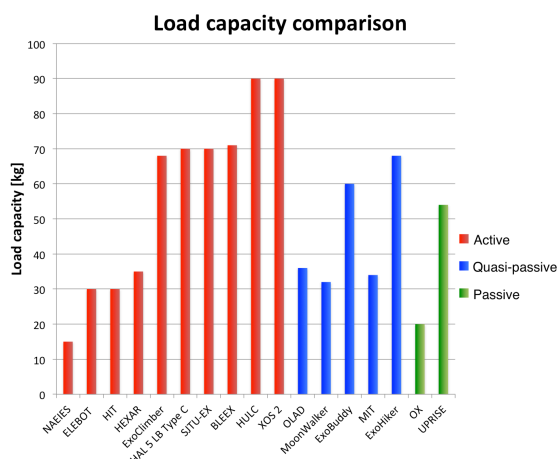
(a) Weight by active DoF



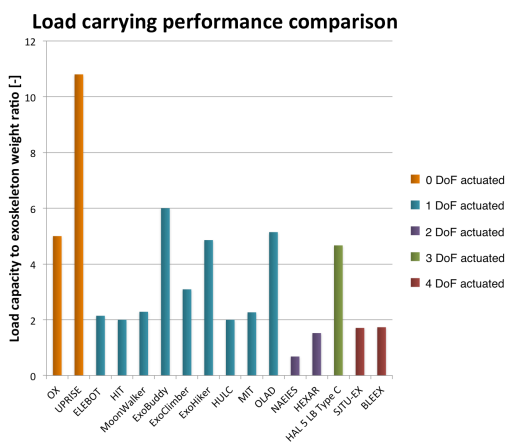
(b) Weight by power source



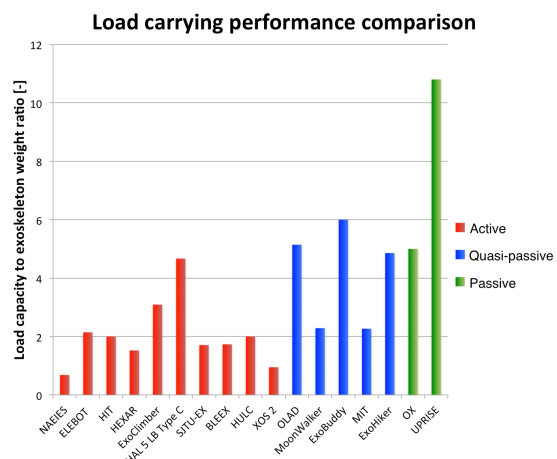
(c) Load capacity by active DoF



(d) Load capacity by power source



(e) Load to weight ratio by active DoF



(f) Load to weight ratio by power source

Figure 3.1: Weight, load carrying capacity and load carrying capacity to weight ratio grouped according to number of actuated DoFs (a, c, e) and power source (b, d, f)

3.3. Discussion

Architecture

The following section discusses the results. From Table 3.2, we observe that the majority of the current exoskeletons have an anthropomorphic architecture. We also observe that exoskeletons increasing joint performance are only present in the anthropomorphic category. As a result of the aligned hip, knee and ankle rotations in the sagittal plane between exoskeleton and user, it is convenient to directly apply torques at the human joints. It also makes the design of exoskeletons simpler, due to the fact that use can be made of data of joint kinematics during gait to design actuators [63]. Furthermore, anthropomorphic exoskeletons generally fit very closely to the user's body, allowing for compact/sleek designs, though the reviewed exoskeletons seem fairly bulky due to the large actuators. Although the rotation axes are aligned in the sagittal plane, other rotation axes such as hip adduction/abduction, hip rotation, ankle inversion/eversion and ankle rotation are generally not due to design simplifications. The misalignment of said rotation axes introduces shear forces during gait, however since the rotations are relatively small, they are often accepted. Another implication of the anthropomorphism of exoskeletons is that they require tight alignment of the joints in the sagittal plane. This in turn means that precise adjustability is necessary to fit different users properly.

Non-anthropomorphic exoskeletons on the other hand do not need to fit the user precisely. Not much research has been done on such exoskeletons, perhaps due to the simplicity and straightforwardness of the design of anthropomorphic exoskeletons.

Weight & load carrying capacity

Figures 3.1a and 3.1b show the weights of the exoskeletons found arranged by number of actuated DoF and power source, respectively. Figure 3.1a gives an indication that the weight of the exoskeleton increases with the number actuated DoF. Although XPED has three actuated DoF, they are passively actuated by springs, explaining the low weight. Figure 3.1b suggests that active exoskeletons generally weigh more. This can be reasoned by the fact that passive elements such as mechanical springs generally weigh less than actuators.

Figures 3.1c and 3.1d present the load carrying capacity of the exoskeletons found arranged by number of actuated DoF and power source. Both figures show that the load carrying capacity is not necessarily dependent on number of actuated DoF or whether the exoskeleton is active, quasi-passive or passive. Exoskeletons with one actuated DoF, such as Exobuddy, ExoClimber, ExoClimber and HULC, are capable of carrying the same amount of load as exoskeletons with multiple actuated DoFs per leg, such as HAL, SJTU-EX and BLEEX. This suggests that more actuators do not necessarily increase load carrying capacity. Care should be taken when reviewing the load carrying capacity of the UPRISE exoskeleton, as it seemingly only supports a weight during stance of the user, where the exoskeleton components are aligned in a straight line to transfer the load effectively to the ground.

Figures 3.1e and 3.1f show the load carrying capacity to exoskeleton weight ratio. Although other factors may play a role in the performance of the exoskeleton, such as ergonomics, power consumption and cost, this ratio is a simple starting point for assessing the performance of each exoskeleton. Here, higher numbers indicate better performance, as the exoskeletons are able to carry more load relative to their own weight. From Figure 3.1e, we conclude that in general exoskeletons with more actuated DoFs perform worse than exoskeletons with few actuated DoFs. The low ratio for exoskeletons with many actuated DoFs can be reasoned by the fact that the actuators are accompanied by extra weight. A similar conclusion can be drawn from Figure 3.1f, where passive and quasi-passive exoskeletons perform better than active exoskeletons, when looking at the load carrying capacity to weight ratio.

Actuation

Electric actuators are used most often in exoskeletons. Hydraulics are also used, however to some smaller extent. Hydraulics are generally used in applications where large amounts of power are necessary, whereas electric actuators are well suited for a wide range of applications. Electric actuators are often more efficient, but heavier than hydraulic actuators [71].

For efficiency reasons, generally not every exoskeleton DoF is actuated. Only the DoFs that require substantial amounts of power are actuated. The rest are equipped with passive elements. To determine which DoFs are to be actuated, gait kinematics are often relied on, to see which DoFs requires most power. During normal gait hip, knee and ankle DoF in the sagittal plane require most power, therefore most exoskeletons these DoFs actuated.

Next to the fact that heavy actuators consume large amounts of energy, they also add mass to the exoskeleton. Studies have shown that added mass increases the metabolic cost of walking [20], especially distal mass [71].

DoF & ergonomics

Most anthropomorphic exoskeletons do not have the same number of DoFs as the human body or have them properly aligned with the human DoFs. This is generally due to design simplifications. The exoskeleton ankle rotational DoF is often not present, because the hip rotational DoF is said to facilitate human ankle rotation.

Little is said on ergonomics of the exoskeletons, however it can be argued that having less DoF than the human body will introduce discomfort for the user. Though braces are useful for keeping the exoskeleton in its correct place relative to the user, it may introduce shear forces due to misalignment issues. Exoskeletons that are minimally connected to the human body (solely at the torso and shoes) are expected to not exhibit this problem.

As a result of the interaction forces between the exoskeleton and the user due to misalignment issues, gait patterns will likely alter, resulting in higher metabolic costs [72].

3.4. Conclusion

A review of the state-of-the-art lower limb exoskeletons for assistance and augmentation has been carried out. The found exoskeletons were categorized according to architecture, power source and intended application. Next, metrics consisting of actuator type, weight, DoF per leg, actuated DoF per leg were extracted. A comparison was made between exoskeletons focusing on load carriage. Therefore lower load carrying capacity was also extracted and the performance of various load carrying exoskeletons was evaluated.

The majority of exoskeletons employed electric or hydraulic actuators. Electric actuators were, logically, solely present in the category of active exoskeletons, whereas hydraulic actuators saw use in both active and quasi-passive exoskeletons. In the case of quasi-passive exoskeletons, they act as dampers. Other actuators included gas springs, gravity balancers and magnetorheological dampers.

It was found that active exoskeletons are generally heavier than passive and quasi-passive exoskeletons. Similarly, exoskeletons with a higher number of actuated DoF are also generally heavier. The large mass and size of active exoskeletons have long been an issue in the adoption of exoskeletons. Though more powerful actuators may be able to carry their own added mass and add power to the user, their inertia remains, rendering such exoskeletons unsuited in dynamic settings.

Less intuitively, quasi-passive and passive exoskeletons, despite having no active actuators, were capable of carrying loads similar to active exoskeletons. Exoskeletons with multiple actuated DoFs also did not seem to be able to carry more load than their counterparts with less actuated DoFs. These are signs indicating that this direction of quasi-passive design and minimal usage of active actuators is promising towards the design of lightweight load carrying exoskeletons.

Little non-anthropomorphic exoskeletons were found to have been developed. Possibly due to the simplicity and straightforwardness of the design of anthropomorphic exoskeletons. However alleviating the anthropomorphic constraint in exoskeleton design opens the door to a very wide range of exoskeleton architectures [31]. A possible benefit could include more efficient load transfer mechanisms, allowing for smaller and lighter actuators. Furthermore, due to the increased freedom in actuator placement, improved dynamic behavior could be achieved. By placing actuators more proximal to the body's centre of mass, lower inertia can be realized. Also, alignment issues greatly reduced, due to the inherent nature of non-anthropomorphic exoskeletons of not having to follow the shape of the human limbs [26]. A drawback may be that since the exoskeleton does not necessarily follow the human limbs, the overall work space might become larger, though this is very dependent on exoskeleton design. Another drawback is that the design space of non-anthropomorphic exoskeletons is incredibly large, requiring a systematic approach for designing such devices.



(a) Agri-robot



(b) BLEEX



(c) CUHK-EXO



(d) ELEBOT



(e) ExoClimber



(f) HAL-5 LB Type C



(g) HEXAR



(h) HULC



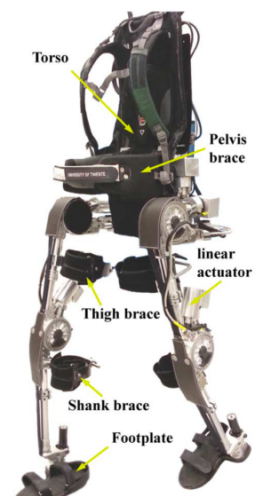
(i) HIT



(j) Indego



(k) KIT



(l) MINDWALKER

Figure 3.2: Images of reviewed exoskeletons

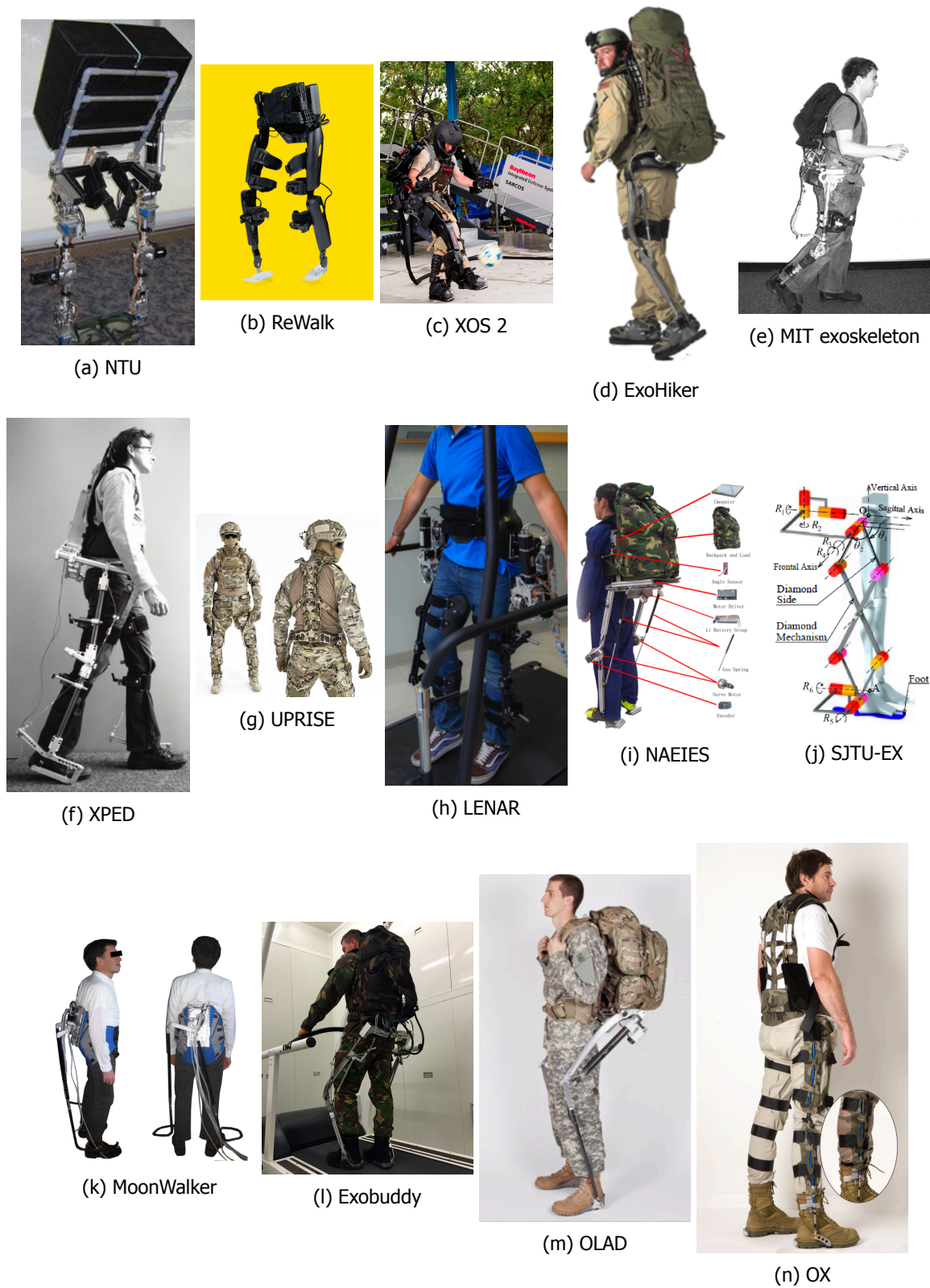


Figure 3.3: Images of reviewed exoskeletons (*continued*)

Bibliography

- [1] M. W. Whittle, *Gait analysis: an introduction*, [Gait Analysis](#) **3**, 223 (2007).
- [2] A. M. F. Barela, P. B. De Freitas, M. L. Celestino, M. R. Camargo, and J. A. Barela, *Ground reaction forces during level ground walking with body weight unloading*, [Brazilian Journal of Physical Therapy](#) **18**, 572 (2014).
- [3] S. A. Birrell, R. H. Hooper, and R. A. Haslam, *The effect of military load carriage on ground reaction forces*, [Gait and Posture](#) **26**, 611 (2007).
- [4] J. Drain, R. Orr, R. L. Attwells, and D. Billing, *Load Carriage Capacity of the Dismounted Combatant - A Commander's Guide*, Dsto-Tr-2765 , 1 (2012).
- [5] J. Knapik, *Load Carriage in Military Operations*, [Review Literature And Arts Of The Americas](#) , 66 (2010).
- [6] S. A. Birrell, *The Biomechanics of Military Load Carriage and Injury Potential*, (2007).
- [7] A. Leardini, C. Belvedere, F. Nardini, N. Sancisi, M. Conconi, and V. Parenti-Castelli, *Kinematic models of lower limb joints for musculo-skeletal modelling and optimization in gait analysis*, [Journal of Biomechanics](#) (2017), 10.1016/j.jbiomech.2017.04.029.
- [8] C. L. Vaughan, [Journal of Biomechanics](#), Vol. 34 (2001) pp. 1107–1115.
- [9] J. Taborri, E. Palermo, S. Rossi, and P. Cappa, *Gait partitioning methods: A systematic review*, [Sensors \(Switzerland\)](#) **16**, 40 (2016).
- [10] J. Dicharry, *Kinematics and kinetics of gait: From lab to clinic*, [Clinics in Sports Medicine](#) **29**, 347 (2010).
- [11] D. A. Winter, *Overall principle of lower limb support during stance phase of gait*, [Journal of Biomechanics](#) **13**, 923 (1980).
- [12] T. H. Paul Devita, Joseph Helseth, *Muscles do more positive than negative work in human locomotion*, **210**, 3361 (2008).
- [13] D. Winter and D. Robertson, *Joint Torque and Energy Patterns in Normal Gait*, [Biological Cybernetics](#) **29**, 137 (1978).
- [14] D. Majumdar, M. S. Pal, and D. Majumdar, *Effects of military load carriage on kinematics of gait*. [Ergonomics](#) **53**, 782 (2010).
- [15] E.-J. Hyung, H.-O. Lee, and Y.-J. Kwon, *Influence of load and carrying method on gait, specifically pelvic movement*. [Journal of physical therapy science](#) **28**, 2059 (2016).
- [16] H. Kinoshita, *Effects of different loads and carrying systems on selected biomechanical parameters describing walking gait*, [Ergonomics](#) **28**, 1347 (1985).
- [17] P. E. Martin and R. C. Nelson, *The effect of carried loads on the walking patterns of men and women*, [Ergonomics](#) **29**, 1191 (1986).
- [18] B. Givoni and R. F. Goldman, *Predicting metabolic energy cost*. [Journal of Applied Physiology](#) **30**, 429 LP (1971).
- [19] K. B. Pandolf, B. Givoni, and R. F. Goldman, *Predicting energy expenditure with loads while standing or walking very slowly*, (1976).

- [20] T. Griffin *et al.*, *Metabolic cost of generating muscular force in human walking: insights from load-carrying and speed experiments*, *J Appl Physiol* **95**, 172 (2002).
- [21] J. Knapik, E. Harman, and K. Reynolds, *Load carriage using packs: A review of physiological, biomechanical and medical aspects*, *Applied Ergonomics* **27**, 207 (1996).
- [22] R. F. Johnson, J. J. Knapik, and D. J. Merullo, *Symptoms during load carrying: effects of mass and load distribution during a 20-km road march*. *Perceptual and motor skills* **81**, 331 (1995).
- [23] C. R. Mahoney, E. Hirsch, L. Hasselquist, L. L. Leshner, and H. R. Lieberman, *The effects of movement and physical exertion on soldier vigilance*, *Aviation Space and Environmental Medicine* **78** (2007).
- [24] L. Awai, M. Franz, C. S. Easthope, H. Vallery, A. Curt, and M. Bolliger, *Preserved gait kinematics during controlled body unloading*, *Journal of NeuroEngineering and Rehabilitation* **14**, 25 (2017).
- [25] J. F. Veneman, *Emerging directions in lower limb externally wearable robots*, *Frontiers Inform Technol Electron Eng* **9184**, 1 (2016).
- [26] A. M. Dollar and H. Herr, *Lower Extremity Exoskeletons and Active Orthoses: Challenges and State-of-the-Art*, *IEEE Transactions on Robotics* **24**, 144 (2008).
- [27] H. Herr, *Exoskeletons and orthoses: classification, design challenges and future directions*, *Journal of NeuroEngineering and Rehabilitation* **6**, 21 (2009).
- [28] A. Zoss, H. Kazerooni, and A. Chu, *On the mechanical design of the Berkeley Lower Extremity Exoskeleton (BLEEX)*, in *2005 IEEE/RSJ International Conference on Intelligent Robots and Systems, IROS* (2005) pp. 3132–3139.
- [29] S. Toyama and G. Yamamoto, *Development of wearable-agri-robot - Mechanism for agricultural work*, *2009 IEEE/RSJ International Conference on Intelligent Robots and Systems, IROS 2009* , 5801 (2009).
- [30] A. Tsukahara, Y. Hasegawa, and Y. Sankai, *Standing-up motion support for paraplegic patient with robot suit HAL*, *2009 IEEE International Conference on Rehabilitation Robotics, ICORR 2009* , 211 (2009).
- [31] D. Accoto, F. Sergi, N. L. Tagliamonte, G. Carpino, and A. Sudano, *A lower limb non-anthropomorphic wearable robot*, (2014).
- [32] W. Van Dijk and H. Van Der Kooij, *XPED2: A passive exoskeleton with artificial tendons*, *IEEE Robotics and Automation Magazine* **21**, 56 (2014).
- [33] H. A. Quintero, R. J. Farris, C. Hartigan, I. Clesson, and M. Goldfarb, *A powered lower limb orthosis for providing legged mobility in paraplegic individuals*, **17**, 25 (2012).
- [34] Mawashi, *UPRISE technology overview*, http://www.mawashi.net/images/Mawashi_{ }UPRISE_{ }Technology_{ }Overview_{ }20170510.pdf (2017), [Online; accessed 2017-12-28].
- [35] S. Wang *et al.*, *Design and Evaluation of the Mindwalker Exoskeleton*, *IEEE transactions on neural systems and rehabilitation engineering : a publication of the IEEE Engineering in Medicine and Biology Society* **4320**, 277 (2014).
- [36] A. Goffer, *Gait-locomotor apparatus*, (2001).
- [37] B. Chen, H. Ma, L. Y. Qin, X. Guan, K. M. Chan, S. W. Law, L. Qin, and W. H. Liao, *Design of a lower extremity exoskeleton for motion assistance in paralyzed individuals*, *2015 IEEE International Conference on Robotics and Biomimetics, IEEE-ROBIO 2015* , 144 (2016), arXiv:1204.3968 .
- [38] H. Cao, Z. Ling, J. Zhu, Y. Wang, and W. Wang, *Design frame of a leg exoskeleton for load-carrying augmentation*, *2009 IEEE International Conference on Robotics and Biomimetics, ROBIO 2009* , 426 (2009).

- [39] H. Kazerooni, *ExoHiker™ by Berkeley Robotics & Human Engineering Laboratory*, <http://bleex.me.berkeley.edu/research/exoskeleton/exohiker/> (2005), [Online; accessed 2017-12-21].
- [40] H. Kazerooni, *ExoClimber™ | Berkeley Robotics & Human Engineering Laboratory*, <http://bleex.me.berkeley.edu/research/exoskeleton/exoclimber/> (2005), [Online; accessed 2017-12-21].
- [41] H. Kazerooni, *Berkeley Robotics & Human Engineering Laboratory (ExoClimber)*, <http://bleex.me.berkeley.edu/research/exoskeleton/hulc/> (2014), [Online; accessed 2017-12-21].
- [42] D. Lim, W. Kim, H. Lee, H. Kim, K. Shin, T. Park, J. Lee, and C. Han, *Development of a lower extremity Exoskeleton Robot with a quasi-anthropomorphic design approach for load carriage*, in *IEEE International Conference on Intelligent Robots and Systems*, Vol. 2015-Decem (2015) pp. 5345–5350.
- [43] C. Zhang, X. Zang, Z. Leng, H. Yu, J. Zhao, and Y. Zhu, *Human-machine force interaction design and control for the HIT load-carrying exoskeleton*, *Advances in Mechanical Engineering* **8**, 1 (2016).
- [44] J. Beil, G. Perner, and T. Asfour, *Design and Control of the Lower Limb Exoskeleton KIT-EXO-1*, *International Conference on Rehabilitation Robotics (ICORR)*, 119 (2015).
- [45] K. Low, X. L. X. Liu, and H. Y. H. Yu, *Development of NTU wearable exoskeleton system for assistive technologies*, *IEEE International Conference Mechatronics and Automation*, 2005 **2**, 1099 (2005).
- [46] L. Gui, Z. Yang, X. Yang, W. Gu, and Y. Zhang, *Design and control technique research of Exoskeleton Suit*, *Proceedings of the IEEE International Conference on Automation and Logistics, ICAL 2007*, 541 (2007).
- [47] C. Koerhuis, F. Krause, and W. V. Dijk, *Exobuddy: een (semi-)passief exoskelet dat de last ondersteunt tijdens langdurige verplaatsingen*, (2017).
- [48] K. W. Hollander, P. Clouse, N. Cahill, A. Boehler, and T. G. Sugar, *Design of the Orthotic Load Assistance Device*, 7th Annual Dynamic Walking Conference, 172 (2012).
- [49] Y. Miao, F. Gao, and D. Pan, *Mechanical design of a hybrid leg exoskeleton to augment load-carrying for walking*, *International Journal of Advanced Robotic Systems* **10** (2013), 10.5772/57238.
- [50] T. W. Chapman, *NoREx DSTO exoskeleton*, https://www.dst.defence.gov.au/sites/default/files/opportunities/documents/ExoSkeleton_fact%20sheet.pdf, [Online; accessed 2017-12-21].
- [51] S. Krut, M. Benoit, E. Dombre, and F. Pierrot, *MoonWalker, a lower limb exoskeleton able to sustain bodyweight using a passive force balancer*, in *Proceedings - IEEE International Conference on Robotics and Automation* (2010) pp. 2215–2220.
- [52] A. B. Zoss, H. Kazerooni, and A. Chu, *Biomechanical Design of the Berkeley Lower Extremity Exoskeleton (BLEEX)*, *IEEE/ASME Transactions on Mechatronics* **11**, 128 (2006).
- [53] *Raytheon XOS 2 Exoskeleton, Second-Generation Robotics Suit*, <http://www.army-technology.com/projects/raytheon-xos-2-exoskeleton-us/>, accessed: 2017-12-25.
- [54] W. Kim, H. Lee, D. Kim, J. Han, and C. Han, *Mechanical design of the Hanyang Exoskeleton Assistive Robot (HEXAR)*, *International Conference on Control, Automation and Systems*, 479 (2014).

- [55] S. Yu, H. Lee, W. Kim, and C. Han, *Development of an underactuated exoskeleton for effective walking and load-carrying assist*, *Advanced Robotics* **30**, 535 (2016).
- [56] A. Zoss and H. Kazerooni, *Architecture and Hydraulics of a Lower Extremity Exoskeleton*, *Mechanical Engineering*, **1** (2005).
- [57] H. Kazerooni, *BLEEX by Berkeley Robotics & Human Engineering Laboratory*, <http://bleex.me.berkeley.edu/research/exoskeleton/bleex/>.
- [58] HAL® THERAPY - CYBERDYNE, <https://www.cyberdyne.jp/english/services/HALTherapy.html> (2008), [Online; accessed 2017-12-05].
- [59] Y. Sankai, *HAL: Hybrid assistive limb based on cybernics*, *Springer Tracts in Advanced Robotics* **66**, 25 (2010).
- [60] *Introduction to Indego*, (2015).
- [61] Parker Hannifin Corp., *Indego – Powering People Forward | Parker Indego*, <http://indego.com/indego/en/home><http://www.indego.com/indego/en/home>, [Online; accessed 2017-12-01].
- [62] *ReWalk 6.0 – Home*, <http://rewalk.com/>, [Online; accessed 2017-11-30].
- [63] A. Valiente and H. Herr, *Design of a Quasi-Passive Parallel Leg Exoskeleton to Augment Load Carrying for Walking by*, (2005).
- [64] C. J. WALSH, K. ENDO, and H. HERR, *A QUASI-PASSIVE LEG EXOSKELETON FOR LOAD-CARRYING AUGMENTATION*, *International Journal of Humanoid Robotics* **04**, 487 (2007).
- [65] A. F. Lafeber, *Reducing human energy expenditure for naturally efficient locomotion using passive support*, (2012).
- [66] W. Van Dijk and H. Van Der Kooij, *XPED2: A passive exoskeleton with artificial tendons*, *IEEE Robotics and Automation Magazine* **21**, 56 (2014).
- [67] Mawashi, *UPRISE: Tactical Exoskeleton*, <http://www.mawashi.net/en/uprise-tactical-exoskeleton> (2017), [Online; accessed 2017-12-28].
- [68] SoldierSystems, *UPRISE Tactical exoskeleton*, <http://soldiersystems.net/2017/07/24/mawashi-uprise-tactical-exoskeleton/> (2017), [Online; accessed 2017-12-28].
- [69] Y. Miao, F. Gao, and D. Pan, *State classification and motion description for the lower extremity exoskeleton SJTU-EX*, *Journal of Bionic Engineering* **11**, 249 (2014).
- [70] K. Mudie, T. Chapman, and D. C. Billing, *Passive exoskeleton to transfer backpack mass to the ground*, *Journal of Science and Medicine in Sport* **20**, S100 (2017).
- [71] A. Zoss and H. Kazerooni, *Design of an electrically actuated lower extremity exoskeleton*, *Advanced Robotics* **20**, 967 (2006).
- [72] B. Maathuis, *XPED 's Reality Check*, (2012).

B

Material choice

Coiling imparts strains on the material, which should remain in the elastic region in order to avoid yielding of the material. Additionally, the material should have a high Young's modulus in order to have good load-bearing properties. However maximising one property will have negative effects on the other, as can be seen from Hooke's law in Eq. (B.1).

$$\epsilon = \frac{\sigma}{E} \quad (\text{B.1})$$

With the desired material properties in mind, we can consult material selection charts for Young's modulus and yield strength [22], shown in Fig. B.1.

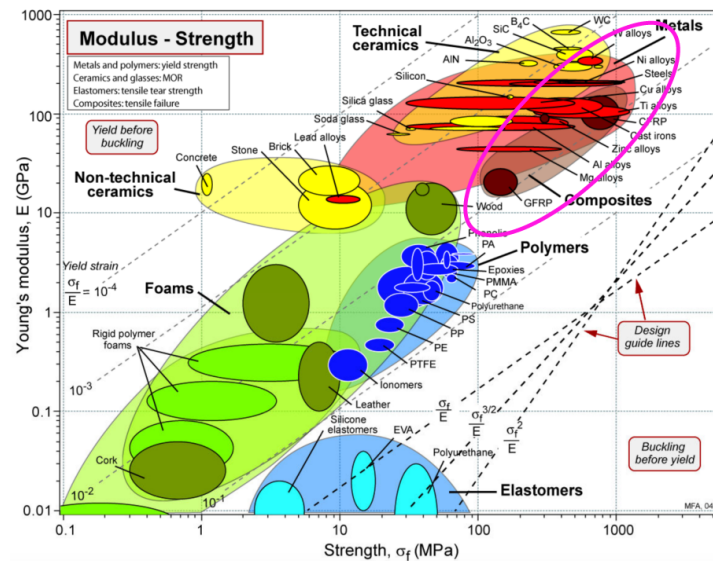
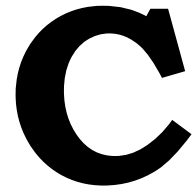


Figure B.1: Material selection chart for Young's modulus and yield strength. Highlighted in purple is the region with suitable materials for the STEM.

The dashed lines represent maximum admissible strains. We aim to find a material with a high Young's modulus and a high maximum admissible strain. The area with suitable materials is indicated with a purple ellipse. We find that the best two candidates are fibre reinforced composites and metals. In prior research, metal tape springs were generally made of spring steel, Beryllium-Copper or titanium [23]. While metals offer higher Young's moduli, composites provide higher admissible strains. Additionally, fibre reinforced composites offer the possibility of tailoring the material properties by using different fibre orientations and lay up configurations. Fibre reinforced composites are also favoured when it comes to the fabrication. Therefore, fibre reinforced composites are chosen as the material for the STEM. Within the domain of fibre reinforced composite materials, many possibilities exist. Generally,

glass, carbon, Kevlar or aramid fibres are used in conjunction with epoxy or polyester resin. Due to the high impact resistance and relatively low cost of glass fibres as opposed to the others, glass is chosen as the fibre material.

Despite the fact that epoxy resin is slightly costlier than polyester, it is safer during handling and has better mechanical properties [24]. Therefore, epoxy resin is chosen.



Composite material model

Composite materials are comprised of at least two distinct materials working together to provide special material properties, essentially forming a “new” material. In the case of fiber reinforced composites, a fibre material and a matrix material are present, where the fibers provide strength and the matrix holds the fibers in place. Fiber reinforced composites offer great flexibility in material properties due the freedom of fiber orientation, lay-up and material choice. Generally, the following properties are available regarding composite materials from the manufacturer:

- E_f : Young’s modulus of fiber material [GPa]
- E_m : Young’s modulus of matrix material [GPa]
- ν_f : Poisson’s ratio of fiber material [-]
- ν_m : Poisson’s ratio of matrix material [-]
- v_f : Fiber volume fraction [-]
- t : Thickness of lamina [m]
- θ : Angle between fiber direction and loading direction [°]

Using the parameters described above, we wish to obtain the properties of the combined material: the fiber reinforced composite. Most commercially available fiber are woven together as it makes handling easier. In an effort to characterise the material properties of any chosen composite, it is convenient to use a model. A simple material model based on classical laminate theory is chosen [24]. In classical laminate theory, a laminate is regarded as a stacked sequence of uni-directional lamina. An uni-directional lamina is a single layer consisting of matrix material and fibers oriented solely in one direction. Stacking multiple lamina (possibly with different fiber orientations) on top of each other results in a laminate. Classical laminate theory uses a number of assumptions, which are summed up below:

- The laminate is constructed from layers of unidirectional lamina
- Weaving of fibers is not taken into account
- All fibers are perfectly straight
- No shearing between layers of lamina
- Perfect bonding between fiber and matrix

Attempts have been made at creating models incorporating the woven characteristic of composites by Soykasap et al. [25], however as extensive material models are out of the scope of this research, it was decided to continue with classical laminate theory. Classical laminate theory computes the material properties of the complete laminate in a bottom-up fashion. The general approach is touched on next.

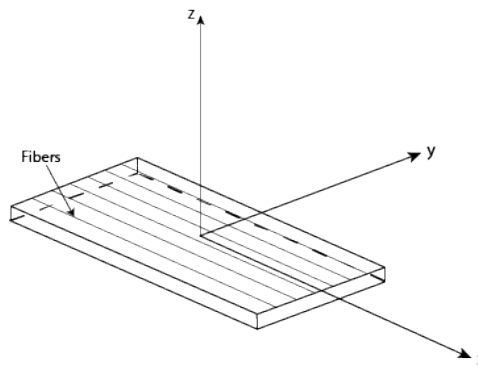


Figure C.1: Fibers oriented parallel to the lamina

- 1. Combining fiber and matrix** The fiber and matrix properties are combined, resulting in the lamina properties. The fibers are oriented parallel to the lamina as shown in Fig. C.1.
- 2. Angles plies** An extra variable is introduced, namely the fiber orientation angle θ , as shown in Fig. C.2. As the fiber orientation is varied, the material properties of the lamina change accordingly. The material properties parallel to and normal to the fibers are transformed into lamina properties (along the x and y directions). The 1, 2, z coordinate system is dependent on the fibers, i.e. the 1 direction is parallel to the fiber, the 2 direction is normal to the fiber and the z direction is the out of plane direction.

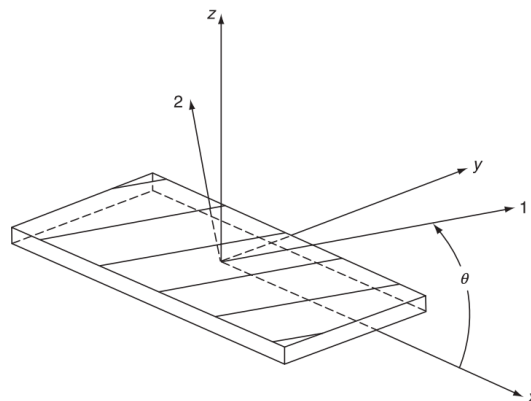
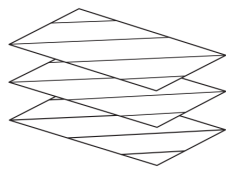


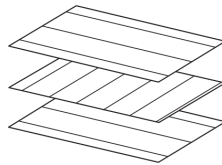
Figure C.2: Fibers oriented at an angle to the lamina

- 3. Stiffness matrices** Having obtained the material properties of the lamina for any arbitrary fiber orientation θ , stiffness matrices are computed for each lamina in order to relate stresses and strains.
- 4. Stacking laminae** Laminae are stacked, and thus their stiffness matrices are combined to result in laminate stiffness matrices. These are the extensional stiffness matrix A, the coupling stiffness matrix B and the bending stiffness matrix D. Together, they relate forces and moments to mid-plane strains and curvatures. A number of stacking examples are shown in Fig. C.3.
- 5. Obtaining properties of the laminate** Using the A, B and D matrices, material properties of the complete laminate can be derived.

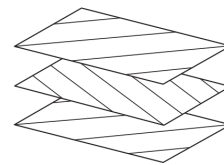
For an in-depth description and the governing equations of classical laminate theory, refer to the book Fiber Reinforced Composites by P.K. Mallick [24].



(a): Uni-directional



(b): Cross ply



(c): Angle ply

Figure C.3: Examples of stacking sequences. (a) shows lamina with the same fibre orientation being stacked, (b) shows lamina with fibre orientations of 0° and 90° in alternating fashion

D

Yielding

When coiling a STEM, significant strain is applied on the material. It is important that the material does not yield when coiled. On the mid-plane of the material, we assume that there are no strains. As we move further away from the mid-plane in the thickness direction, the strain increases linearly. We consider a thin plate of thickness t subject to pure bending. We define u, v and w as the deflections in the x, y and z directions, as shown in Fig. D.1.

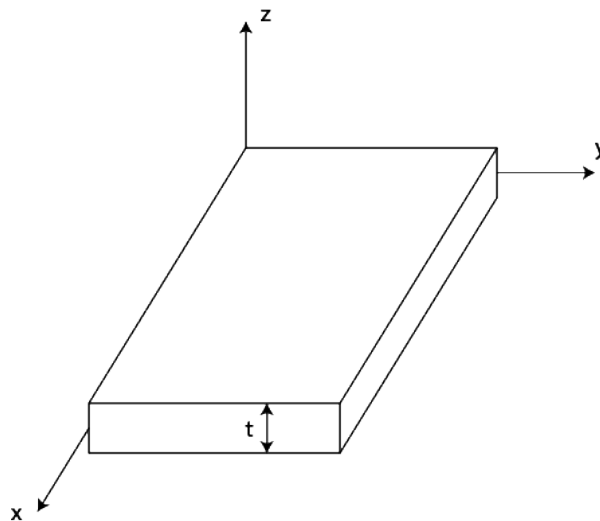


Figure D.1: Schematic of a plate element along with its axes

The deflections at any point P within the plate are given by Eqs. (D.1) and (D.2).

$$u = -z \frac{\delta w}{\delta x} \quad (\text{D.1})$$

$$v = -z \frac{\delta w}{\delta y} \quad (\text{D.2})$$

The relationships between the deflections (u and v) and strains (ϵ_x and ϵ_y) are given by Eqs. (D.3) and (D.4).

$$\epsilon_x = \frac{\delta u}{\delta x} \quad (\text{D.3})$$

$$\epsilon_y = \frac{\delta v}{\delta y} \quad (\text{D.4})$$

Combining Eqs. (D.1) through (D.4), yields Eqs. (D.5) and (D.6).

$$\epsilon_x = -z \frac{\delta^2 w}{\delta x^2} \quad (\text{D.5})$$

$$\epsilon_y = -z \frac{\delta^2 w}{\delta y^2} \quad (\text{D.6})$$

, where $-\frac{\delta^2 u}{\delta x^2}$ and $-\frac{\delta^2 v}{\delta y^2}$ are the curvatures κ_x and κ_y , respectively. κ_x is the longitudinal curvature and κ_y is the transverse curvature (refer to Fig. 3.2). We can write the curvatures as:

$$\kappa_x = \frac{1}{r_x} \quad (\text{D.7})$$

$$\kappa_y = \frac{1}{r_y} \quad (\text{D.8})$$

During bending, the largest strains occur on the outer most layers (at $z = \pm \frac{t}{2}$). Filling this value in for z result in Eqs. (D.9) and (D.10).

$$\epsilon_x = \pm \frac{t}{2r_x} \quad (\text{D.9})$$

$$\epsilon_y = \pm \frac{t}{2r_y} \quad (\text{D.10})$$

ϵ_x and ϵ_y should remain below the maximum allowable strain of the used material. For composites, we choose the material (fiber or matrix) which has the lowest allowable strain. Furthermore, the sign of the strains do not matter. Thus we can define a critical ratio between thickness and bending radius of the STEM which has to be satisfied at all times (Eqs. (D.11) and (3.3)).

$$\frac{t}{2r_x} < \epsilon_{\max} \quad (\text{D.11})$$

$$\frac{t}{2r_y} < \epsilon_{\max} \quad (\text{D.12})$$



Natural coiling radius

Deforming any material elastically stores energy. When a STEM is coiled, it stores energy and will assume a configuration in which its stored energy is at its lowest state.

Eq. (E.1) relates moments with induced curvature changes in the bending of a plate, through the D matrix, obtained from the material model presented in Appendix. C.

$$\begin{bmatrix} M_x \\ M_y \end{bmatrix} = \begin{bmatrix} D_{11} & D_{12} \\ D_{21} & D_{22} \end{bmatrix} \begin{bmatrix} \Delta\kappa_x \\ \Delta\kappa_y \end{bmatrix} \quad (\text{E.1})$$

The expression for pure bending of a thin plate is given by Eq. (E.2) [26].

$$dU = -\frac{1}{2}(M_x \frac{\delta^2 w}{\delta x^2} + M_y \frac{\delta^2 w}{\delta y^2}) dx dy \quad (\text{E.2})$$

, where

$$-\frac{\delta^2 w}{\delta x^2} = \Delta\kappa_x = \frac{1}{r_x} \quad (\text{E.3})$$

$$-\frac{\delta^2 w}{\delta y^2} = \Delta\kappa_y = \frac{1}{r_y} \quad (\text{E.4})$$

Combining Eqs. (E.1) through (E.4), we get the following expression for dU in Eq. (E.5).

$$dU = \frac{1}{2}(D_{11}\Delta\kappa_x^2 + D_{22}\Delta\kappa_y^2 + 2D_{12}\Delta\kappa_x\Delta\kappa_y) dx dy \quad (\text{E.5})$$

Integrating Eq. (E.5) yields the following expression for the total energy U , given in Eq. (E.6).

$$U = \frac{1}{2}(D_{11}\Delta\kappa_x^2 + D_{22}\Delta\kappa_y^2 + 2D_{12}\Delta\kappa_x\Delta\kappa_y)A \quad (\text{E.6})$$

, where A is the area of the STEM that has undergone deformation, and can thus be expressed as given in Eq. (E.7)

$$A = r_x \alpha r_y \theta \quad (\text{E.7})$$

Here α is the subtended angle of the STEM, which is 2π (a full tube) and θ is the bend angle in radian. Filling in Eq. (E.7) into Eq. (E.6) yields Eq. (E.8).

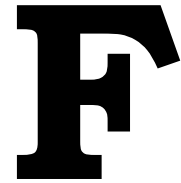
$$U = \frac{1}{2}(D_{11}\Delta\kappa_x^2 + D_{22}\Delta\kappa_y^2 + 2D_{12}\Delta\kappa_x\Delta\kappa_y)r_x \alpha r_y \theta \quad (\text{E.8})$$

Tidying up and differentiating this expression with respect to r_x results in Eq. (E.9).

$$\frac{dU}{dr_x} = \frac{\alpha\theta}{2} \left(-\frac{D_{11}r_y}{r_x^2} + \frac{D_{22}}{r_y} \right) \quad (\text{E.9})$$

Equating this expression to zero to find a minimum energy configuration yields Eq. (3.4).

$$r_{xn} = \sqrt{\frac{D_{11}}{D_{22}}} r_y \quad (\text{E.10})$$



Spring Choice

In order to obtain a compact system, the balancing spring will take on the form of a torsion spring acting on the drum. To this end we first convert the force-displacement characteristic to a torque-rotation characteristic, which is done by multiplying the force at each instance with the corresponding radius of the coil. The result, shown in Fig. F.1, is a fairly constant torque-rotation profile, suggesting that a constant torque spring is a fitting solution.

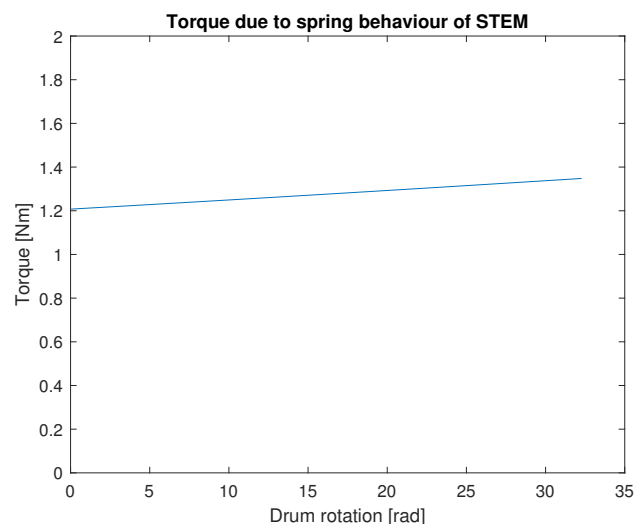


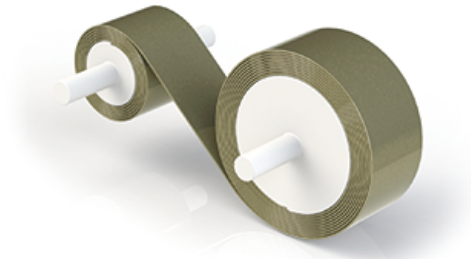
Figure F.1: Torque generated on the drum by the spring behaviour of the STEM. The STEM is fully extended at 0 rad and fully compressed at 32 rad.

A constant torque spring, shown in Fig. F.1(b) is an extension of the simple, classical constant force spring, shown in Fig. F.1(a). Based on the torque requirement, a constant torque spring by Hunter Spring and Reel (product no. 20012) came closest to what was desired. Its dimensions are given in Table F.1. Refer to Fig. 3.9 for an accompanying image explaining the dimensions.

The result of balancing the torque characteristic out with the mentioned spring is shown in Fig. F.3(a). The net torque curve is then transformed back to a force-displacement curve in Fig. F.3(b). The STEM is not completely balanced, however the values are sufficiently small that no discomfort will be experienced by the user.



(a): An example of a constant force spring. Image courtesy of Amazon [?].



(b): An example of a constant torque spring. By winding the free end of the spring onto a secondary drum, the constant force spring is transformed into a constant torque spring. Image courtesy of Vulcan [?].

Figure F.2: Examples of constant force and torque springs.

Table F.1: Dimensions of the chosen constant torque spring with product number 20012 from Hunter Spring and Reel.

Dimension	Value
Torque (Nm)	1.02
Storage drum D2 (mm)	38.86
Output drum D3 (mm)	67.82
Storage flange D1 (mm)	62.2
Output flange D4 (mm)	84.33
Center to Center S (mm)	84.33
Thickness T (mm)	0.3
Width W (mm)	19.05

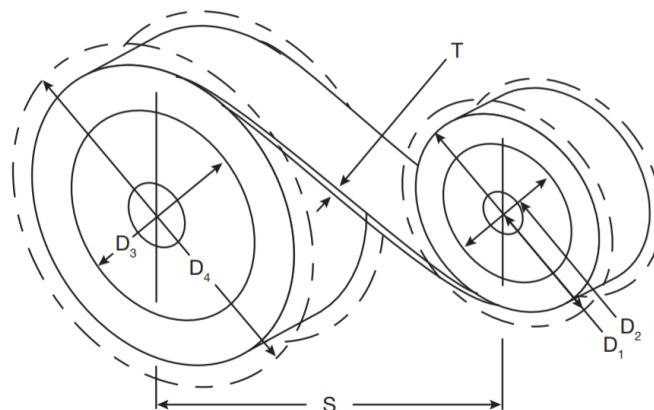
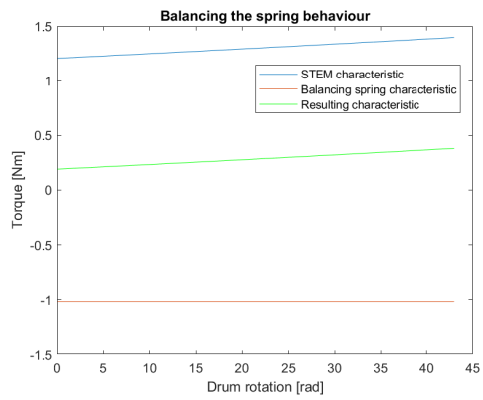
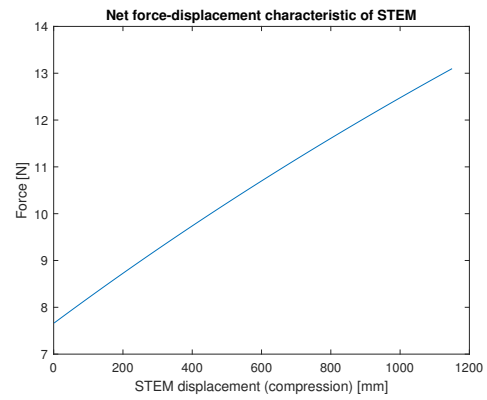


Figure F.3: A schematic of a constant torque spring along with its relevant dimensions.



(a): The torque characteristic is balanced by means of a constant torque spring.



(b): The resulting characteristic is transformed into a force-displacement curve.



STEM Fabrication

A list of materials and tools used for the fabrication of the STEM is shown below.

- Priming wax
- PVA film
- Glass fibre sleeve, 45mm diameter
- Epoxy resin L + Hardener EPH500
- Shrink sleeve, 139mm width
- PVC tube, 50mm outer diameter, 2m
- Mixing cups
- Pipe stand
- Mixing sticks
- Paintbrushes
- Dustcap
- Latex gloves
- Sanding paper
- Heat gun
- Tape
- Kitchen scale

The procedure is described next. A dustcap and safety gloves were worn at all times during the fabrication process. Fig. [G.1](#) shows a number of pictures in the fabrication process.

1. Irregularities on the surface of the PVC pipe are sanded. A cardboard sheet is placed underneath and the pipe is set up between two pieces of ITEM profile such that the middle part is cleared from the ground.
2. Two layers of priming wax are applied to the surface of the tube using paper towels. Then two layers of PVC film are applied. During each layer, 5-10 minutes is waited for the layers to dry.
3. The glass fibre sleeve is put over the pipe and fixed at the ends using tape. The amount of necessary resin is calculated. As a rule of thumb, 750g of resin for every m^2 of glass fibre is necessary. The resin and hardener are mixed in a 100:63 ratio.

4. The resin mixture is brushed onto the glass fibre sleeve until it is completely impregnated with resin.
5. A shrink sleeve is pulled over the pipe, taking care that the fibres are not moved.
6. A heat gun is used to shrink the shrink sleeve. The pipe is heated from one end to the other end, squeezing any excess resin out.
7. The packed pipe is left to cure for at least 24 hours, after which the shrink sleeve is torn off.
8. A dremel is used to a slit in the tube along the length. Then the STEM can be removed from the PVC pipe. Approximately 5cm from the ends of the STEM are cut off to smooth out the edges.



(a): The glass fibre sleeve is fixed onto the PVC mould



(b): The shrink sleeve is pulled over the impregnated glass fibre sleeve.



(c): The STEM after curing and removing from the mould. The ends remain to be cut.

Figure G.1: Stages in the fabrication process

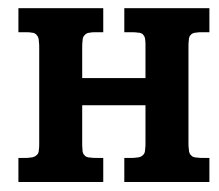
The properties of the glass fibre and resin are given in Tables G.1 and G.2, respectively. This specific resin type was chosen out of a wide range of resin types due to the fact that it has good mechanical properties and cures at room temperature. Some resins possess even better mechanical properties, however they are required to cure at high temperatures.

Property	Value
Diameter range	10 to 60 mm
Thickness	0.27 mm
Weight	37 g/m
Diameter at 45° fiber angle	45 mm
E-modulus	73Gpa
Poisson's ratio ν	0.18
Fiber volume fraction v_f	0.6
Density ρ	2.6g/cm ³
Tensile strength σ_{TS}	3.4GPa
Allowable strain	3.5%

Table G.1: Properties of E-fiberglass sleeve (from Carbonwinkel.nl)

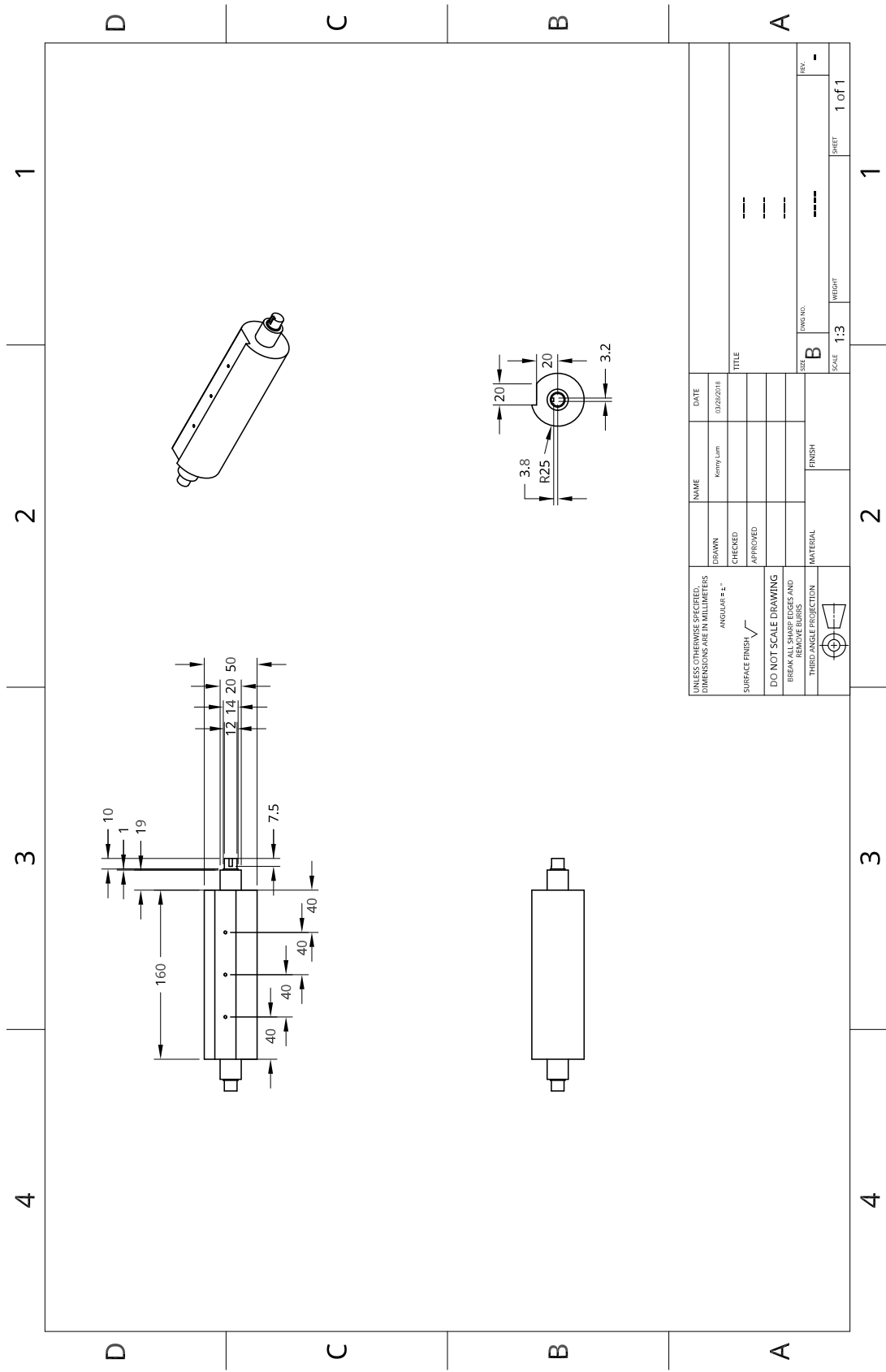
Property	Value
Tensile strength	68MPa
Allowable strain	2%
E-modulus	2.93GPa
Mixing ratio	100:63 resin to hardener
Processing time	60minutes
Curing temperature	25C°
Curing time	24hours

Table G.2: Properties of L + EPH500 epoxy resin (from Carbonwinkel.nl)

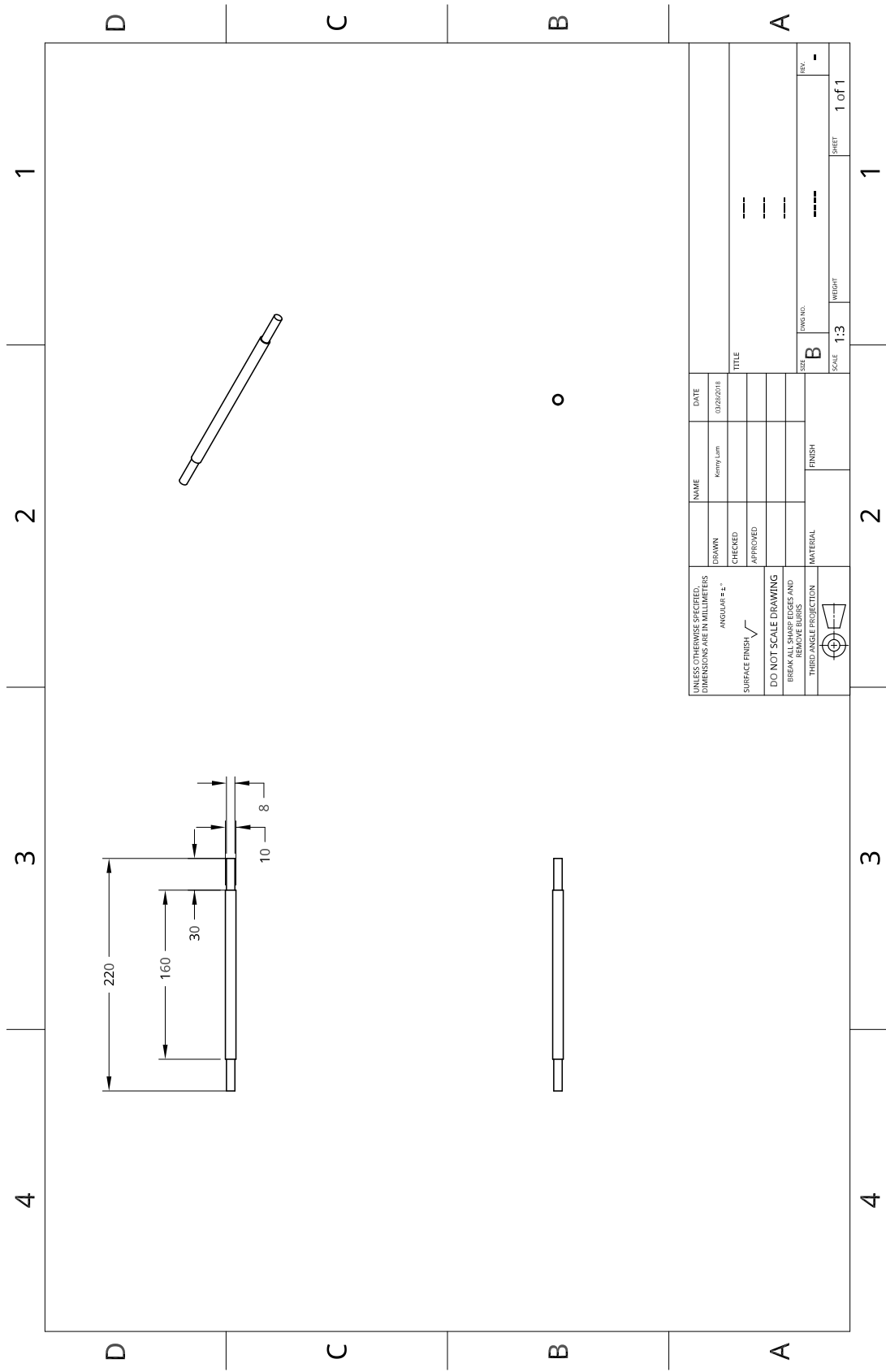


Technical Drawings

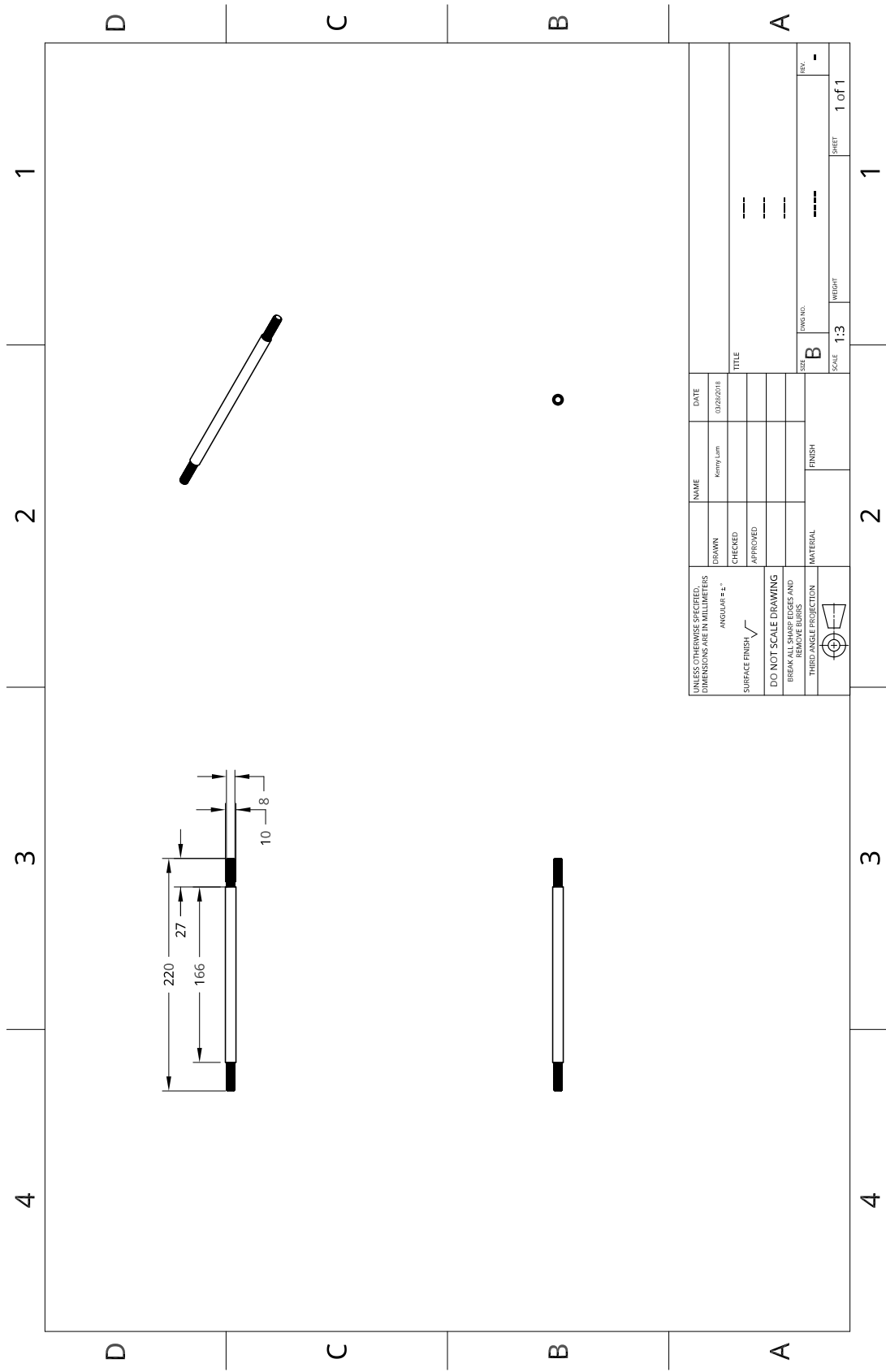
H.1. Coiling Drum Drawing



H.2. Guidance Roller Drawing



H.3. Spacer Rod Drawing



H.4. Side Plate Drawing

